Grafting Polyacrylamide from the Surface of Activated Carbon for Flocculation Applications

A Thesis Submitted to the Committee on Graduate Studies in Partial Fulfillment of the Requirements for the Degree of Master of Science in the Faculty of Arts and Science

TRENT UNIVERSITY
Peterborough, Ontario, Canada

Materials Science M.Sc. Graduate Program
May 2023

Abstract

Grafting Polyacrylamide from the Surface of Activated Carbon for Flocculation Applications

Sarah J. Bégin

The generation of polymer brushes by surface-initiated polymerization techniques has become a powerful tool for the creation of hybrid materials. Governed by the type and amount of polymer used in the modification, the chemical and physical properties of a surface can be tailored by polymer grafting. In this study, a commonly used polymer flocculant, polyacrylamide (PAM), was grafted onto the surface of activated carbon (AC). This hybrid material was designed with the intent of combining the functionalities of both the activated carbon and the polymer flocculant, potentially acting in a synergistic manner. The PAM grafted AC (AC-PAM) was examined as a flocculant in the treatment of mature fine tailings (MFT).

AC-PAM was synthesized by surface-initiated activators generated by electron transfer atom transfer radical polymerization (SI-AGET ATRP). This was accomplished by pre-functionalizing the surface of activated carbon by oxidation, followed by the attachment of an ATRP initiator. From this surface, SI-AGET ATRP of acrylamide monomers was performed. The resulting AC-PAM was characterized by FTIR, XPS, TGA, SEC, and BET analysis. Characterization results indicated the successful grafting of polyacrylamide from the surface of activated carbon. The AC-PAM was measured to contain approximately 10.6% PAM by weight, and the average-number molecular weight of the grafted polymer was 176,100 g/mol. The flocculation performance of AC-PAM

and PAM were compared by performing settling tests with 5 wt% MFT. The optimal polymer dosage for PAM was found to be 10,000 ppm, producing an initial settling rate of 3.51 m/hr and a supernatant turbidity of 430 NTU. Comparatively, the optimal dosage for AC-PAM was found to be 20,000 ppm, producing a supernatant turbidity of 114 NTU and a fast initial settling rate of 27.54 m/hr. The improved flocculation performance is hypothesized to occur due to the effective increase in the molecular weight of PAM when grafted from the surface of activated carbon. In all, our work demonstrates the successful grafting of PAM from AC, as well as potential wastewater treatment applications for these types of hybrid materials.

Keywords

Activated carbon, polyacrylamide, surface-initiated polymerization, grafting, atom transfer radical polymerization, mature fine tailings, flocculation

Acknowledgments

First and foremost, I would like to thank my supervisor Dr. Andrew Vreugdenhil for his continuous support, advice, and patience throughout the completion of this thesis. The past few years have been a wonderful experience and I am forever grateful for all the opportunities it has brought me. A special thanks goes out to Oliver Strong and Dr. Kevin Scotland for all their help, advice, and technical expertise throughout my studies. I would also like to thank everyone at the Trent Inorganic Materials Research Laboratory, including Kelly Wright, Kyle Fisher, Kyle Reyes, Tyler Roy, Elmira Nazari, and Hamant France. Additionally, I would like to thank Paul Pede from Carbonix Inc. for his support throughout this research. Thank you as well to my committee members Dr. Olena Zenkina and Dr. Carlo Bradac for their inputs over the course of this work. Finally, I would like to express my gratitude to my family and friends for their encouragement and support throughout my studies.

Table of Contents

List of Figures

List of Tables

List of Equations

List of Abbreviations and Symbols

Abbreviations

AC	Activated Carbon
SI	Surface-Initiated
RDRP	Reversible-Deactivation Reactivation Polymerization
MWD	Molecular Weight Distribution
ATRP	Atom Transfer Radical Polymerization
NMP	Nitroxide-Mediated Polymerization
RAFT	Reversible Addition-Fragmentation Chain Transfer Polymerization
AGET ATRP	Activator Generated by Electron Transfer ATRP
ARGET ATRP	Activators Regenerated by Electron Transfer ATRP
TFT	Thin Fine Tailings
MFT	Mature Fine Tailings
OSPW	Oil Sands Process-Affected Water
VOCs	Volatile Organic Compounds
CT	Consolidate Technology
PT	Paste Technology
PAM	Polyacrylamide
P(AM-*co*-AA)	Poly(acrylamide-*co*-acrylic acid)
HPAM	Hydrolyzed Polyacrylamide
P(AM-*co*-DADMAC)	Poly(acrylamide-*co*-diallyl dimethyl ammonium chloride)
XPS	X-ray Photoelectron Spectroscopy
XRF	X-ray Fluorescence
BE	Binding Energy
BET	Brunauer-Emmett-Teller
SEC	Size Exclusion Chromatography
GPC	Gel Permeation Chromatography
GFC	Gel Filtration Chromatography
RID	Refractive Index Detector
PEO/PEG	Polyethylene oxide/Polyethylene glycol
ISR	Initial Settling Rate
FAU	Formazin Attenuation Units

Symbols

Đ	Dispersity
R_p	Rate of Polymerization
k_p	Rate Constant of Propagation
P_n^*	Propagating Radicals
M	Monomer
DP_n	Degree of Polymerization
M_n	Number-Average Molecular Weight

M_w	Weight-Average Molecular Weight
P_n-X	ATRP Dormant Species
Cu^I/L	ATRP Activator
X-Cu^{II}/L	ATRP Deactivator
k_{act}	Rate Constant of Activation
k_{deact}	Rate Constant of Deactivation
k_t	Rate Constant of Termination
K_{ATRP}	ATRP Equilibrium Constant
E_k	Kinetic Energy of a Photoelectron
$h\nu$	Energy of a Photon
Φ	Work Function of Spectrometer
$n_m{}^a$	BET Monolayer Capacity
n^a	Quantity of gas adsorbed
p/p^o	Relative Pressure
C	BET Constant
A_s	BET Surface Area
a_s	BET Specific Surface Area
a_m	Molecular Cross-Sectional Area
V_e	Elution Volume
V_0	Void Volume
V_i	Pore Volume
V_t	Total Liquid Volume
K_{SEC}	SEC Equilibrium Constant
n	Refractive Index of a Dilute Solution
n_0	Refractive Index of Solvent
n’	Refractive Index of Sample
M_p	Peak Molecular Weight

1. Introduction

1.1 Activated Carbon (AC)

Activated carbon (AC) is a porous carbonaceous material widely used for the adsorption of contaminants from gases and liquid solutions. ACs can be produced by the carbonization of raw materials followed by activation to develop the porous structure.[1] During the carbonization process, most of the non-carbon elements such as oxygen, hydrogen, nitrogen, and sulfur are removed, and the residual carbon atoms arrange themselves to form a microcrystalline structure composed of disordered aromatic sheets. The disorder in the microcrystalline layers is due to the presence of residual heteroatoms and defects such as vacant lattice sites in the carbon sheets.[2] This disorder prevents the sheets from stacking perfectly parallel, thereby leading to empty spaces between these sheets.[3] These empty spaces give rise to the porous structure of AC, which is further enhanced during the activation process when the spaces are cleared of tar and other carbonaceous material produced during the carbonization process.[2] The pores created can be of various sizes and are often classified according to their pore widths. Micropores are defined as pores with widths less than 2 nm, mesopores have widths in the range of 2-50 nm, and macropores have widths greater than 50 nm.[4] The highly developed pore structure of ACs lead to their large surface areas, typically with surface areas in the range of 800 – 1500 m^2/g.[2]

In addition to the porous structure and large surface areas of ACs, the high adsorption capacity of the material is influenced by the chemical structure of the carbon surface. Due to the presence of heteroatoms such as oxygen, hydrogen, and nitrogen, a variety of functional groups can be found on the surface of AC (Figure 1.1).[5,6] The concentration of

these heteroatoms and functional groups is determined by the nature of the starting material and activation method used to produce the AC, as well as any post-activation surface modifications performed. These functional groups heavily influence the properties of the AC such as hydrophobicity, surface charge, electron density of the graphene layers, and may also be used as reactive points for further surface modifications.[7]

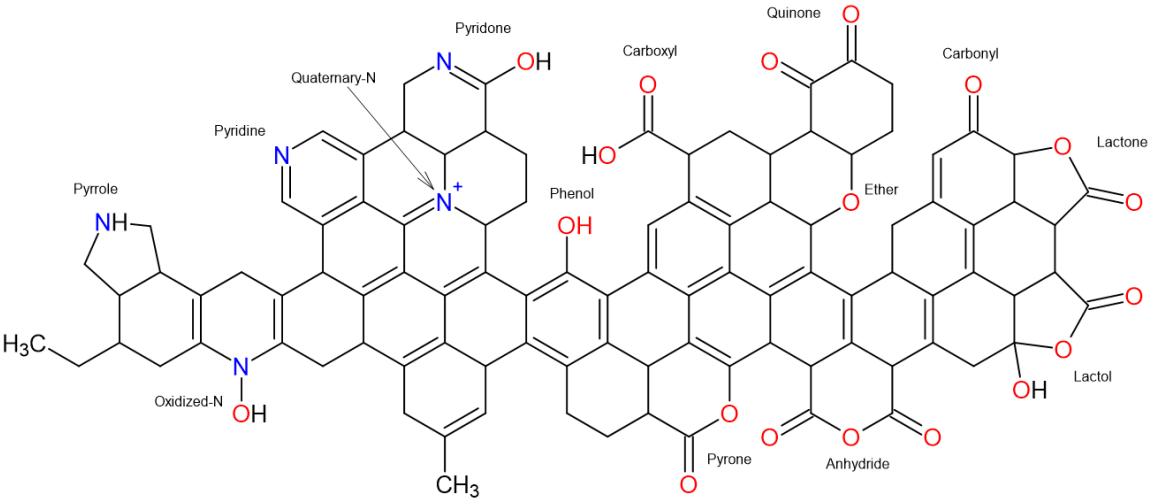

Figure 1.1 *– Potential oxygen and nitrogen containing functional groups on the surface of activated carbon*

Oxygen containing functional groups such as carboxyl, anhydride, lactone, lactol, and phenol impart an acidic behaviour to the AC. These functional groups can provide sites for the selective adsorption of metal ions/metal complexes from solutions.[5] Other oxygen containing functional groups such as carbonyl, quinone, ether, and pyrone are considered either neutral or weakly basic in nature. Other basic functional groups include nitrogen containing functional groups such as pyrrole, pyridine, pyridone, and quaternary-N.[6] Basic functional groups have been shown to improve the adsorption of organics such as phenols by ACs.[8]

A variety of surface modification techniques such as oxidation, sulfuration, and ammonification can be used to alter the concentration of functional groups on the surface of AC.[9] In addition to affecting the surface chemistry and adsorptive properties of ACs,

these functional groups can be used as building blocks for the attachment of organic molecules onto the surface of AC. Compared to other modification methods such as impregnation, covalent modifications do not suffer the drawback of potential leaching of the grafted molecule. Carbonaceous materials such as activated carbon are ideal supports due to their high surface areas, allowing for a high degree of functionalization.[10] In this work, the covalent attachment of polymers onto the surface of AC is explored as a surface modification technique for AC. Due to the repeated chain structure, polymer molecules can impart a high degree of functionality on the surface of AC. Depending on the functional groups present in the grafted polymer, the AC-polymer hybrid could be used for a variety of environmental applications.

1.2 Polymer Brushes

Among the various surface modification techniques available, polymer modified AC is of particular interest. Modification by polymer grafting can be used to tailor the chemical and physical properties of a substrate such as, surface wettability, electronic properties, colloidal stability, adsorption capacities, thermal stability, etc.[11–14] A variety of substrates have been used for polymer grafting, including graphene, carbon nanotubes, metals, metal oxides, proteins, etc.[13–16] Polymers that are covalently anchored to a surface are commonly referred to as polymer brushes. Polymer brushes can be formed by either a *grafting to*, *grafting from*, or *grafting through* approach (Figure 1.2). In the grafting to approach, polymers are grafted by reacting end-functionalized polymer chains with an appropriately functionalized substrate.[17] However, this method does not allow for the formation of dense polymer brushes due to the steric repulsion between polymer chains, as well as chemisorption of the polymer chains onto the surface.[14,17] Typically, higher

grafting densities can be achieved using a grafting from approach, where the chains are directly grown from an initiator functionalized surface.[17] In this bottom-up approach, polymer brushes can be grown by a variety of surface-initiated reversible-deactivation radical polymerization (SI-RDRP) techniques. A grafting through method is also described in the literature, where polymer brushes are grown from a surface functionalized with polymerizable groups. In this case, polymer chain initiation can take place in solution or in bulk, where monomers can propagate from the polymerizable group on the surface of the substrate. However, this process also produces non-grafted polymer chains. Additionally, the length and density of the grafted chains are more difficult to control in this method.[14] For these reasons, my work is focused on the development of polymer brushes on activated carbon using the grafting from approach.

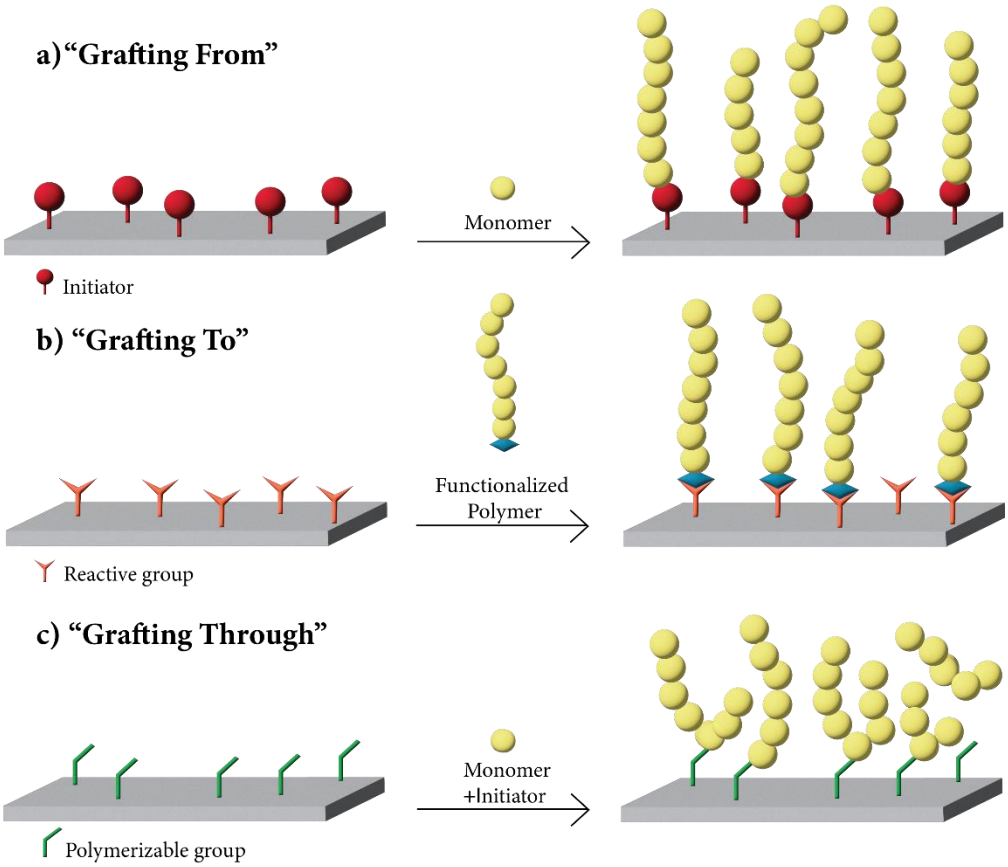

Figure 1.2 *- Formation of polymer brushes by (a) grafting from, (b) grafting to, and (c) grafting through strategy*

1.3 Reversible-deactivation radical polymerization (RDRP)

Reversible-deactivation radical polymerization (RDRP), also known as controlled/living radical polymerization, is a polymerization technique capable of forming polymers with relatively low dispersity (Đ) values and allows for the precise control over polymer molecular weight, architecture, and composition.[18] These features are inaccessible to conventional free radical polymerization techniques due to fast rates of termination and chain transfer reactions.[19] RDRP provides control over the polymerization by establishing a dynamic equilibrium between a low concentration of propagating radicals and a dormant species. The insertion of periods of dormancy increases the lifetime of the growing chains and reduce the rate of termination reactions, thereby allowing for slow but simultaneous growth of all chains.[20]

The most commonly used RDRP techniques include atom transfer radical polymerization (ATRP), reversible addition-fragmentation chain transfer polymerization (RAFT), and nitroxide-mediated polymerization (NMP). In ATRP and NMP, the dynamic equilibrium between propagating radicals and dormant species is achieved by trapping radicals in a deactivation/activation process. Propagating radicals are trapped in a deactivation process by a stable radical such as a nitroxide (as in NMP) or an alkyl halide species (as in ATRP). The dormant species can be activated either spontaneously or by a catalyst (as in ATRP) to reform the propagating radicals. Since the persistent radicals cannot terminate with each other but only reversibly react with the growing radicals, the concentration of growing radicals is reduced and the rate of termination reactions between growing radicals is minimized.[19] Comparatively, in the RAFT process, the dynamic equilibrium between propagating radicals and a dormant species is accomplished by highly efficient chain transfer reactions. In this case, a free chain radical

releases a trapped chain radical from its end-capped species and becomes end-capped itself. Since this exchange process is highly efficient, the rate of termination reactions is minimized.[21]

1.3.1 Features of Reversible-Deactivation Radical Polymerization

RDRP should display first-order kinetic behavior, pre-determinable degree of polymerization, low dispersity, and long-lived polymer chains with preserved end functionalities.[22] The rate of polymerization (R_p) can be given by Equation 1,

$$R_p = -\frac{d[M]}{dt} = k_p[M][P_n^*] \quad (1)$$

where k_p is the rate constant of polymerization, [M] is the concentration of monomer, and $[P_n^*]$ is the concentration of growing radicals.[23] The first-order kinetic behaviour arises from the negligible contribution of non-reversible termination reactions, making the concentration of growing radicals essentially constant. Therefore, the polymerization kinetics can be described by Equation 2,

$$ln\frac{[M]_0}{[M]} = k_p\,[P_n^*]t = k_p^{app}t \quad (2)$$

where k_p^{app} is the apparent rate constant of polymerization when $[P_n^*]$ is constant.[23]

RDRP procedures display pre-determinable degrees of polymerization (DP_n) due to efficient initiation and a constant number of chains maintained throughout the reaction. The degree of polymerization (DP_n) can be predicted by the ratio of the concentrations of consumed monomer [M] and initiator initially introduced $[I]_0$, Equation 3.[19]

$$DP_n = \frac{\Delta[M]}{[I]_0} = \frac{[M]_0}{[I]_0}\,x\ monomer\ conversion \quad (3)$$

The theoretical molecular weight of a polymer can be calculated from the degree of polymerization by simply multiplying DP_n by the molar mass of the monomer unit. Polymers produced by RDRP should have narrow molecular weight distributions (MWD) with low dispersity (Đ, also know as polydispersity or the polydispersity index). Dispersity is defined as the ratio between the weight-average molecular weight (M_w) and the number average molecular weight (M_n). A dispersity value of 1 would represent a perfectly monodisperse polymer sample where all the polymer chains are of the same length.[19] Polymers made by free radical polymerization typically have larger dispersity values in the range of 1.5-2, while those made from RDRP are typically in the range of 1.01-1.5.[19,23]

Finally, polymers formed by RDRP should have long-lived polymer chains with preserved end-functionalities. This is due to the negligible occurrence of irreversible termination and chain transfer reactions, resulting in the polymers retaining their active centers after full monomer consumption. This feature allows for the preparation of block copolymer by pausing the polymerization, adding a second monomer, and re-starting the polymerization to grow the 2nd block.[23]

1.3.2 Atom-Transfer Radical Polymerization (ATRP)

Among the various RDRP techniques, atom transfer radical polymerization (ATRP) is the most widespread technique used to produce polymer brushes.[11] As mentioned above, ATRP establishes a dynamic equilibrium between propagating radicals (P_n^*) and dormant

species (P_n-X), predominantly in the form of initiating alkyl halide/macromolecular species (Figure 1.3).

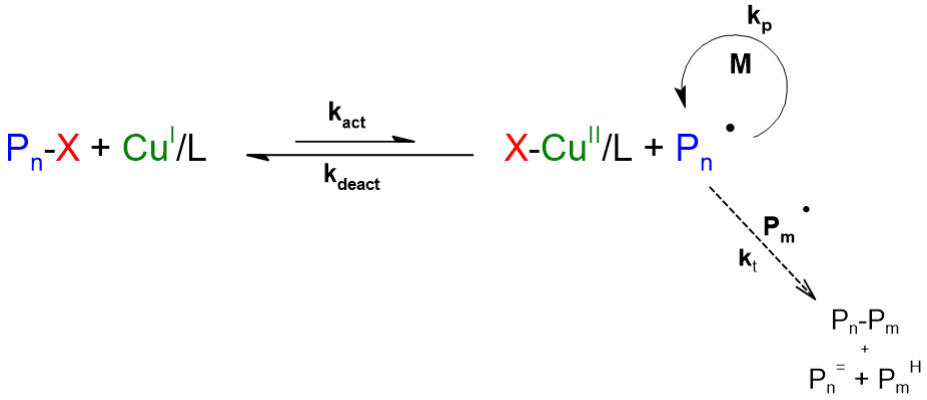

Figure 1.3 *– General mechanism of atom transfer radical polymerization (ATRP)*

The dormant species periodically reacts with a transition metal complex (typically copper) in its lower oxidation state (Cu^I/L) with a rate constant of activation (k_{act}). This forms the higher oxidation state metal complex coordinated with a halide ligand (X-Cu^{II}/L) and a radical species capable of propagating with a rate constant of propagation (k_p) The radical species can also react with the X-Cu^{II}/L with a rate constant of deactivation (k_{deact}) to reform the Cu^I/L complex and dormant species. The ATRP equilibrium constant (K_{ATRP}) can be described by the ratio of k_{act} and k_{deact} and is given by Equation 4,

$$K_{ATRP} = \frac{k_{act}}{k_{deact}} = \frac{[X-Cu^{II}/L][P_n^*]}{[Cu^I/L][P_n-X]} \quad (4)5$$

where [X-Cu^{II}/L] is the concentration of deactivator species, [Cu^I/L] is the concentration of activator species, and [P_n-X] is the concentration of dormant species. Equation 4 can be rearranged in terms of the concentration of propagating radicals and substituted into Equation 1, giving an expression for the rate of polymerization in ATRP (Equation 6).

$$R_p = k_p[M][P_n^*] = k_p K_{ATRP}[M]\left(\frac{[P_n - X][Cu^I/L]}{[X - Cu^{II}/L]}\right) \quad (5)$$

As indicated by Equation 5, to maintain a consistent rate of polymerization, the ratio of Cu^I/Cu^{II} in the system should be maintained. However, due to the occurrence of irreversible radical termination reactions, there is a build up in Cu^{II} species over time. This results in the ratio of Cu^I/Cu^{II} and the rate of polymerization to decrease over time. To prevent the conversion of nearly all the catalyst into Cu^{II} species, relatively high concentrations of metal catalyst (1000-10,000 ppm) are used in "normal" ATRP.[24] In a "normal" ATRP reaction, the transition metal catalyst is introduced in its lower oxidation state to initiate the polymerization. However, due to the low oxidative stability of these complexes, careful handling techniques are required. Additionally, the reaction mixture must be carefully deoxygenated using techniques such as the freeze-pump thaw process.[25] This is particularly difficult in aqueous polymerization solutions, resulting in poor control over the polymerization.[26] The oxygen sensitivity of "normal" ATRP can be overcome using a catalyst in its higher oxidation state in addition to a chemical reducing agent, such as ascorbic acid, to generate the lower oxidation state catalyst in situ (Figure1.4).[25] In this process named activators generated by electron transfer (AGET) ATRP, the oxygen sensitivity of the reaction is reduced by using a more oxidatively stable transition metal complex and through the reduction of any oxygen in the reaction flask.

AGET was a precursor to activators regenerated by electron transfer (ARGET) ATRP, which allows for the total concentration of catalyst to be reduced in comparison to "normal" ATRP (Figure 1.4).[27] Excess chemical reducing agent can be added to convert the Cu^{II} species that builds up due to irreversible termination reactions back into the Cu^I species. Since the ratio of Cu^I/Cu^{II} is maintained and the rate of polymerization is not

dependent on the total concentration of Cu, the concentration of catalyst used can be reduced to < 50 ppm. This process is considered a green procedure in comparison to "normal" ATRP due to the lower concentration of catalyst and reduced oxygen sensitivity.[18]

1.4 Polymer Modified Activated Carbon

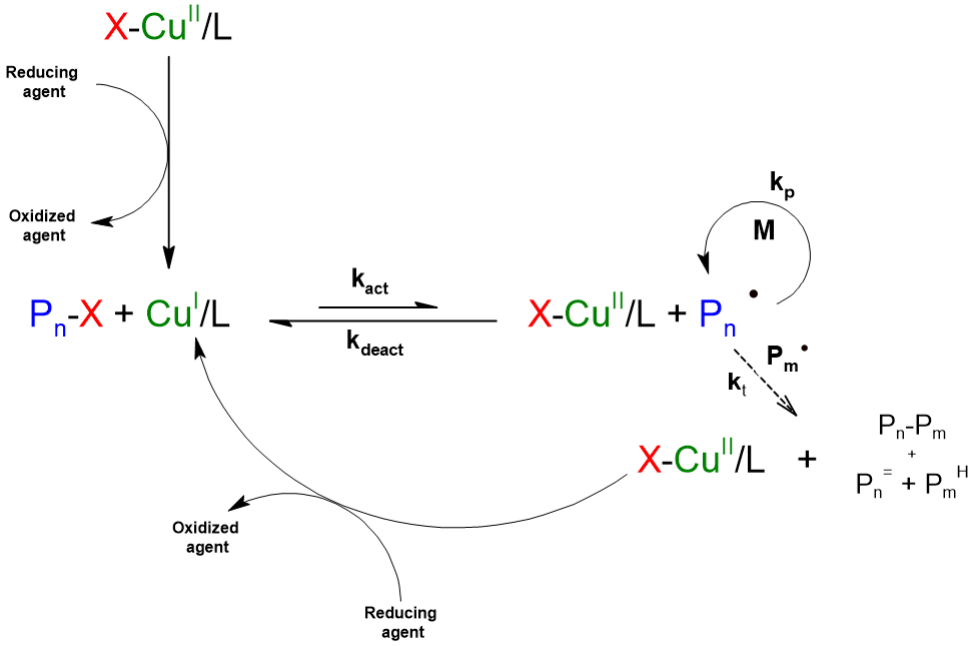

Figure 1.4 *- Activator generated by electron transfer (AGET) ATRP and activators regenerated by electron transfer (ARGET) ATRP*

While a variety of carbon-based materials such as graphene and carbon nanotubes have been used for polymer grafting, there are surprisingly few reports on the use of activated carbon as a substrate for polymer grafting. Utilizing a grafting through approach, a group has reported the synthesis of various "covalent organic polymer" functionalized ACs.[28–31] In this approach, the surface of AC was pre-functionalized by oxidation, followed by acyl chlorination. Melamine monomers were then grafted to the surface of AC, providing potential sites for the polycondensation of other monomer units. However, in this grafting through approach, control over the polymer molecular weight and architecture is limited. A grafting from approach was first developed by Liu and

Wang, where SI-ATRP of hydroxyethyl acrylate was performed.[32] In this approach, the surface of activated carbon was pre-functionalized by oxidation, followed by the attachment of an ATRP initiator. From the initiator functionalized surface, polymers such as poly(hydroxylethyl acrylate) and poly(*N*-isopropylacrylamide) were grown from the surface of AC.[33–35] Similarly, activator generated by electron transfer atom transfer radical polymerization (AGET ATRP) has been utilized for the surface-initiated polymerization of methyl methacrylate and *tert*-butyl acrylate from AC.[36]

1.5 Application – Flocculation of Mature Fine Tailings

Located in the province of Alberta, the Canadian oil sands represent the third largest proven oil reserves in the world, following Venezuela and Saudi Arabia. It was estimated that the Canadian oil sands contain 177 billion barrels of proven reserves, representing approximately 10% of the total proven global reserves. In 2021, Alberta produced crude bitumen at a rate of almost 3.3 million barrels per day.[37] Depending on how deep the oil sands reserves are below the surface, different techniques can be used to extract the bitumen.[38] *In situ* extraction techniques are used when the deposits are too deep for open-pit mining (>75 m). These techniques involve injecting steam into wells drilled through the oil sands deposit, making the bitumen more fluid, which is then pumped to the surface.[38] Open-pit mining, or surface mining, is used when the oil sands deposits are closer to the surface. In this method, oil sands ore is mined, crushed, and mixed with a combination of hot water, steam, and caustics (Clark Hot Water Extraction process).[39] The slurry is pumped to an extraction plant and placed into primary separation vessels where the bitumen is separated from the coarse fraction. Bitumen is recovered as a froth composed of approximately 60% bitumen, 30% water, and 10% mineral solids.[40] The

bitumen froth is then transported to a froth treatment plant, where the froth is further processed to remove fine solids. While bitumen recoveries range from 88-95%, this extraction process also produces large volumes of aqueous waste tailings containing sand, silt, clay, and residual bitumen.[39]

1.5.1 Tailings and Tailings Management

The oil sands tailings are transported to structures called tailings ponds to facilitate the gravitational separation of the solids from water. Once deposited in the tailings ponds, the coarse sand and about one half of the fines (particles <44 um) settle to the bottom of the pond. The remaining fluid fraction is called thin fine tailings (TFT) and is composed of approximately 8% solids by weight.[39] As the suspension settles over time, some of the entrapped water is released and is collected at the top of the pond to be recycled.[41] After consolidation for a few years, the tailings settle to about 30-35% solids and are referred to as mature fine tailings (MFT).[39] The clay particles in MFT remain dispersed and do not undergo significant consolidation over time, forming a stable gel-like suspension.[41] The fine clays are responsible for the slow consolidation of MFT due to their high water retention and negative surface charges. Due to the electrostatic repulsion between the negatively charged clay particles, MFT display colloidal stabilization. This electrostatic repulsion is enhanced by the alkaline pH (pH ~ 8.5) of the MFT, further increasing the colloidal stability. Since MFT do not undergo significant consolidation over time, long term storage in tailings ponds is required. Currently, the ever-growing inventory of tailings ponds in Canada cover an area of over 200 km^2 of land.[42]

In addition to occupying a large area of land, tailings ponds contain large volumes of entrapped water that cannot be recycled for further extraction processes. The long-term

storage of tailings also poses several environmental and health concerns, including the seepage of oil sands process-affected water (OSPW) into surrounding groundwater. Due to the elevated levels of naphthenic acids, inorganics, and metals, seepage of OSPW into groundwater is of concern to nearby communities and wildlife. Additionally, there are environmental concerns over the emission of volatile organic compounds (VOCs) from the tailings ponds.[43] To address these concerns, the Energy Resource Conservation Board in Alberta put in place tailings management regulations for oil sands operators. The objective of these regulations is to ensure that all tailings produced during the life of a project are ready to be reclaimed within ten years after the end of the mining operation.[43–45] While current dewatering technologies can recover about 70% of the water from the oil sands tailings, 3.3 m^3 of tailings are still being produced per 1 m^3 of bitumen extracted. Therefore, if the tailings management regulations are to be met, the existing dewatering technologies need to be improved.[41]

While several techniques have been proposed for the dewatering of MFT, few have been proven on a commercial scale. Consolidate tailings (CT) is a dewatering process used by the industry where the MFT is mixed with a coagulant aid (typically gypsum) and coarse sand. This mixture is deposited in tailings ponds where the sand and clay particles aggregate and release entrapped water. However, due to the use of inorganic coagulants in this process, there is a high concentration of ions such as calcium in the recovered water. Since the presence of calcium makes the recovery of bitumen from oil sands more difficult, the recovered water cannot be used for further extraction procedures.[41] Another dewatering technology practiced by the industry is paste technology (PT). Paste technology utilizes polymer flocculants to rapidly thicken the oil

sands tailings to approximately 25-30 wt% solids. Due to the rapid thickening in this process, the recovered water is still warm and can be readily reused in the bitumen extraction process. However, the sediments formed after PT still contain large volumes of water that cannot be recovered. This limitation is attributed to quality of flocculants currently available, which will be further discussed below.

1.5.2 Flocculation Mechanism

Flocculation can be defined as the aggregation of solids in a colloidal suspension due to the bridging of particles through high molecular weight polymers. Before flocculation can occur, the polymer must first adsorb onto the surface of some of the particles. Depending on the nature of the polymer and particles, adsorption can occur through hydrogen bonding, electrostatic interaction, hydrophobic interaction, and ion bridging.[46] Polymer adsorption can occur when there is a collision between a polymer molecule and a particle in the suspension. The rate of polymer adsorption is dependent on several factors such as the concentrations of particles and polymer molecules, the size of particles and polymer molecules, mixing conditions, viscosity of the suspension, etc. When there is a high concentration of particles in the suspension, the rate of polymer adsorption is high, occurring almost instantaneously. However, for more dilute suspensions, polymer adsorption can take significantly longer. Adsorbed polymer chains attach to the surface in trains and can form loops of polymer extended into the solution. At the end of the chains, long segments of polymer tails can extend into the solution (Figure 1.5A).[47] Adsorbed polymers can destabilize a colloidal suspension by two major mechanisms: bridging

flocculation and charge neutralization. In bridging flocculation, if the adsorbed polymer tail is long enough to extend its segments into the solution at least twice the length of the electrical double layer of the particle, the polymer will likely adsorb onto the surface of more than one particle (Figure 1.5B).[46] In this case, particles are linked together via a high molecular weight polymer, which can further aggregate to form flocs. If too large of a polymer dose is added to the suspension, the particles will have a large adsorption density and will not be accessible for bridging flocculation. Therefore, an optimum dosage should exist to give maximum flocculation performance.[47] Generally, the most effective polymer flocculants regarding polymer bridging are linear, high molecular weight polymers. Linear polymers with higher molecular weights will have long polymer chains that can adsorb onto the surface of multiple particles, resulting in faster settling rates.[41]

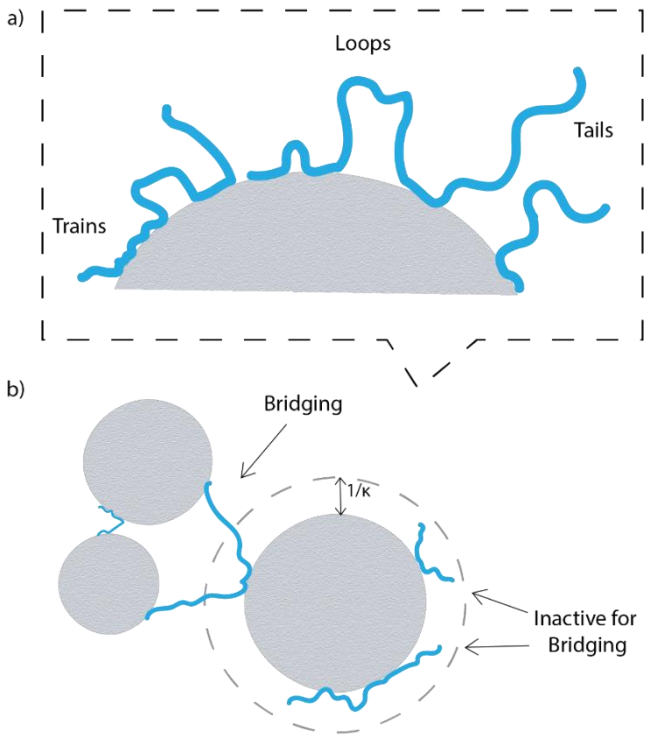

Figure 1.5 *- a) Polymer adsorption onto clay particles forming trains, loops, and tails b) Mechanism for bridging flocculation*

Polyelectrolytes can also promote the aggregation of particles by means of charge neutralization. In the case of polyelectrolytes with the same charge as the suspended particles, the charged polymers compress the thickness of the electrical double layer of

the particles, thereby allowing them to aggregate due to van der Waals attractive forces.[46] For polyelectrolytes with the opposite charge as the suspended particles, the polymer can adsorb onto the surface of the particle by electrostatic attraction, resulting in patches of opposite charge on the surface of the particle. Uncovered particles and particles with patches of opposite charge can also aggregate by means of electrostatic attraction.[47] In both cases, destabilization by charge neutralization is technically considered coagulation and not flocculation. However, in the case of polyelectrolytes, flocculation can occur due to both bridging flocculation and charge neutralization.[46] In addition to polymer dosage, the charge density of the polyelectrolyte is a key factor in flocculation performance.

1.5.3 Flocculants for Paste Technology

Most of the current paste technologies rely on the use of polyacrylamide (PAM) based flocculants for the dewatering of oil sands tailings. PAM based flocculants are typically used since the polymer is water soluble and can easily be synthesized up to high molecular weights.[46] Non-ionic, anionic, and cationic polyacrylamides have been explored for the flocculation of oil sands tailings (Figure 1.6). Non-ionic polyacrylamides adsorb onto the surface of the suspended particles by the formation of hydrogen bonds between the polymer's acrylamide protons and the oxygen atoms on the surface of the particle.[41] Anionic

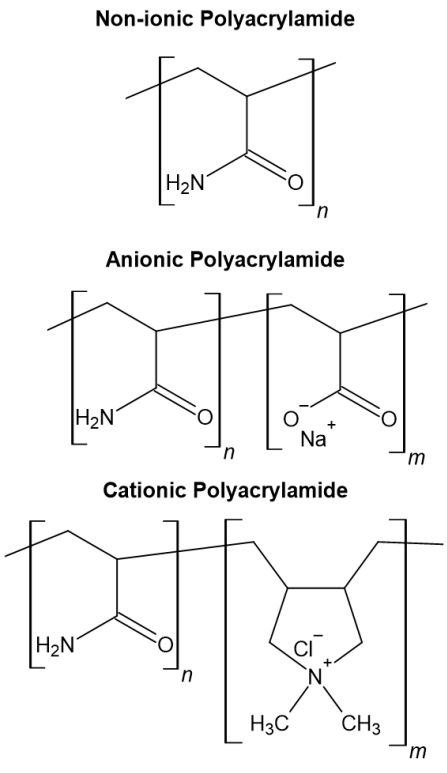

Figure 1.6 *– Chemical structure of non-ionic, anionic, and cationic polyacrylamide (PAM)*

polyacrylamides can be made by either the copolymerization of acrylamide and acrylic acid (P(AM-*co*-AA)) or the partial hydrolysis of polyacrylamide.[42] For anionic polyelectrolytes, intramolecular electrostatic repulsion between the charged polymer segments cause the polymer chain to adopt an extended conformation. In this extended conformation, the polymer chains can adsorb onto the neutral sites of the clay particles and aggregate via bridging flocculation.[46] The flocculation performance can be improved by first treating the tailings with a coagulant to help overcome the repulsive forces between particles.[41] Cationic polyacrylamides are typically made by the copolymerization of acrylamide (AM) and diallyl dimethyl ammonium chloride (DADMAC) (P(AM-*co*-DADMAC)). Cationic polyelectrolytes adsorb onto the surface of the negatively charged particles by means of electrostatic attraction. Particles can agglomerate by means of electrostatic interaction between the local positive charge on the surface of the particle and the negative surface charge of another particle.[41]

While these various polyacrylamide-based flocculants can induce flocculation, they were not optimally designed for the dewatering of oil sands tailings. These commercial flocculants were originally designed for other applications and result in the formation of loosely packed flocs with high water content. These flocs still need to be contained in tailings ponds and contain a large volume of water that cannot be recycled. Therefore, the search for a new polymer flocculant specifically designed to overcome these issues is critical to enhance the dewatering performance of polymer flocculants for oil sands tailings.[41]

2. Key Experimental Techniques

2.1 Key Characterization Techniques

2.1.1 X-Ray Photoelectron Spectroscopy (XPS)

X-ray photoelectron spectroscopy (XPS) is a surface characterization technique used to determine the elemental composition, empirical formula, chemical state, and electronic state of the elements present within a material. In this technique, the surface of a material is irradiated with X-ray photons, which causes the emission of electrons from the material. The emitted electrons (photoelectrons) are a result of a complete energy transfer between the X-ray photons and inner shell electrons from the sample. After the emission of a photoelectron, there is a "hole" created in the orbital in which the electron was removed. This hole is quickly filled by an electron from another orbital accompanied with either the release of energy (X-ray fluorescence) or an "Auger" electron (Figure 2.1).[48]

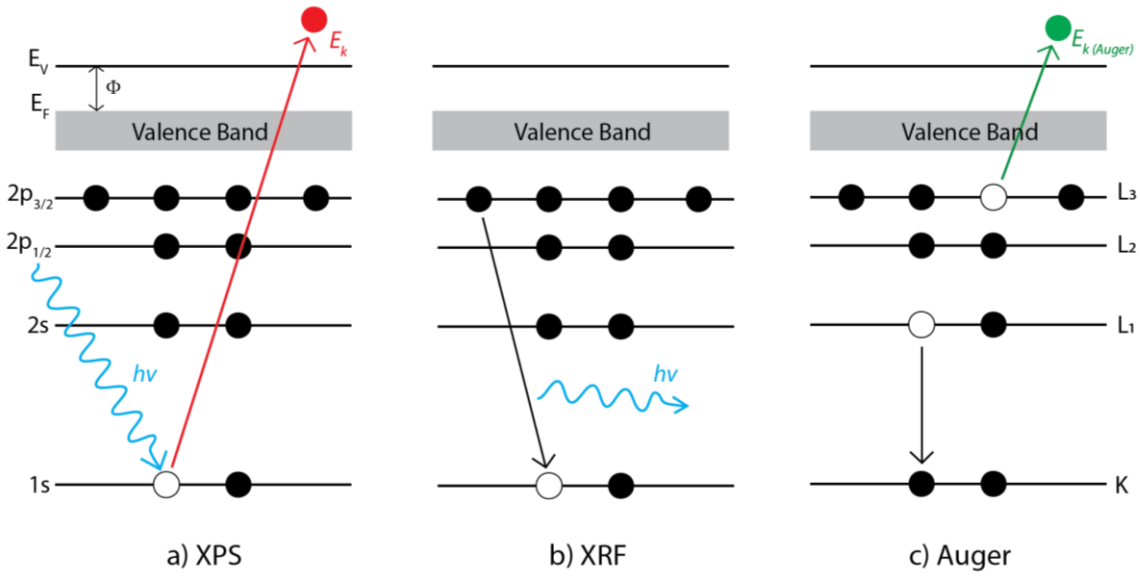

Figure 2.1 *– Energy level diagram for a) X-ray photoelectron emission, b) X-ray fluorescence emission, c) Auger electron emission*

In XPS, the kinetic energy of the photoelectrons can be measured and can be described by Equation 7,

$$E_k = hv - \Phi - BE \quad (6)$$

where hv is the energy of the photon, Φ is the work function of the spectrometer, and BE is the binding energy of the electron. The work function of the spectrometer is the minimum thermodynamic work needed to remove an electron from the surface of a solid. The energy difference between the Fermi level and vacuum level correspond to the work function.[48]

By rearranging equation 1, the binding energy of the emitted photoelectron can be calculated from the measured kinetic energy. The binding energy of an electron will depend on the element and chemical environment from which the electron was ejected. The relative abundance of the various elements in the sample can be determined from the XPS survey scan, which is a plot of the intensity (counts per second) vs. binding energy (eV) of the emitted electrons.

Since the binding energy of photoelectron is also dependent on the chemical environment of the electron, information about the oxidation state of the element and the type of neighboring atoms can also be determined by XPS analysis. In the case of the C 1s

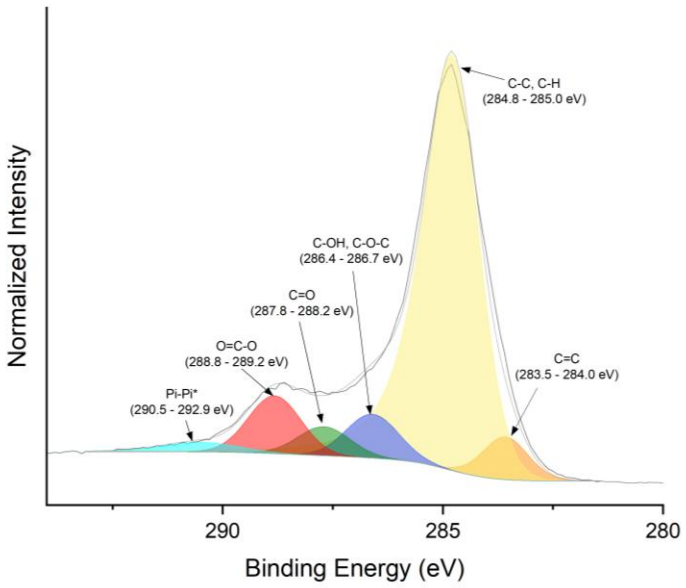

Figure 2.2 – *XPS high-resolution C 1s peak with synthetic components fitted*

photoelectron, the binding energy is highly dependent on the electronegativity of the nearest neighbor elements. As the electronegativity of the neighboring atoms increases, the binding energy of the C 1s photoelectrons also increases.[48] For these reasons, XPS peaks such as C 1s can be fitted with synthetic components and quantified to determine the relative number of carbon atoms in each chemical environment (Figure 2.2).[48]

In this work, all XPS measurements were performed on a Kratos AXIS supra spectrometer using monochromatic Al K(alpha) source (15mA, 15kV). The instrument work function was calibrated to give a binding energy (BE) of 83.96 eV for the Au 4f7/2 line for metallic gold and the spectrometer dispersion was adjusted to give a BE of 932.6 eV for the Cu 2p3 eV line of metallic copper. The Kratos charge neutralizer system was used on all samples. Survey scan analyses were carried out with an analysis area of 300 x 700 microns and a pass energy of 160 eV. High resolution analyses were carried out with an analysis are of 300 x 700 microns and a pass energy of 20 eV. Analysis of the survey scans and high-resolution scans were performed using CASA XPS (version 2.31), with spectra being corrected to the main line of the C1s spectrum at 284.8 eV. Baseline corrections were made by using a Shirley type background correction.

2.1.2 Brunauer-Emmett-Teller (BET) analysis

When a solid surface is exposed to a gas, after an initially large rate of adsorption, an equilibrium between the rate of adsorption and desorption is reached. If the temperature is kept constant during this process, the position of this equilibrium will depend on the pressure of the system.[2] This can be measured using a volumetric method where a known quantity of gas is added to the adsorbent at a constant temperature. At the equilibrium pressure (p), the amount of gas adsorbed (n^a) is calculated from the difference between

the amount of gas admitted and the amount required to fill the space. By plotting the amount of gas adsorbed vs. the equilibrium relative pressure (p/p^o) of the gas at a constant temperature, an adsorption isotherm can be generated.[49] Adsorption isotherms can be used in the determination of the surface area of an adsorbate, pore volume, pore size distribution, heat of adsorption, etc.[2] According to IUPAC, the majority of physisorption isotherms can be grouped into the six types of isotherms shown in Figure 2.3. The reversible *Type I(a) and I(b)* isotherms are characterized by a quick rise in adsorption at low p/p^o values, followed by a plateau as p/p^o approaches 1. This isotherm shape is indicative of monolayer formation and is typically seen in microporous solids with relatively small external surfaces. The steep rate of adsorption at low p/p^o is from micropore filling, where a faster rate is observed with materials having mainly narrow micropores compared to materials with wider micropores and possibly narrow mesopores.[50] The reversible *Type II* isotherm shape is often obtained with non-porous or macroporous adsorbents, where there is unrestricted monolayer-multilayer adsorption. In this isotherm, monolayer adsorption is said to occur up until

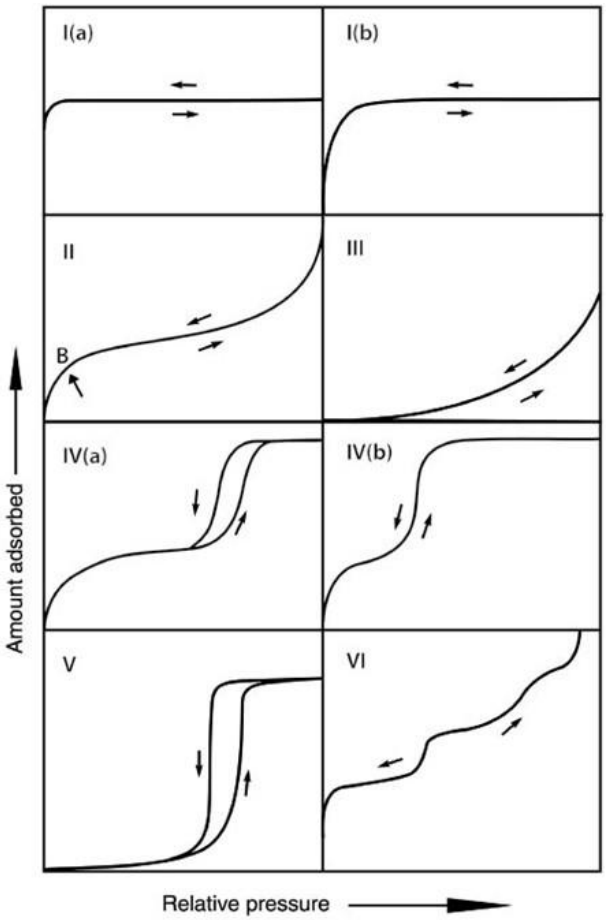

Figure 2.3 *- IUPAC 6 types of isotherms. Image retrieved from ref [58]*

point “B” on the graph, followed by the onset of multilayer adsorption.[50] The reversible *Type III* isotherm has a convex shape to the p/p^o axis, indicating weak adsorbate-adsorbate interactions. In this case, no monolayer is formed as the adsorbate molecules are clustered around the most favorable sites on the surface of a nonporous or microporous solid.[50] *Type IV* isotherms are given by mesoporous adsorbents, characterized by the presence of a hysteresis loop. At first, a monolayer-multilayer is adsorbed on the mesopore walls, followed by capillary condensation. Capillary condensation occurs when the gas condenses to a liquid-like phase in a pore, resulting in multilayer adsorption from the liquid-like phase.[50] *Type V* isotherms have a similar shape to the *Type III* isotherms in the low p/p^o range where there are relatively weak adsorbent-adsorbate interactions. In this case, as p/p^o is increased, molecular clustering is followed by pore filling.[50] *Type VI* isotherm represents stepwise, multilayer adsorption on a uniform and non-porous surface.[49]

The Brunauer-Emmett-Teller (BET) equation is commonly used to evaluate the isotherm data to provide quantitative information about the surface area.[49] The BET equation assumes monolayer adsorption, where the linear form of the equation is used to derive the BET monolayer capacity (n_m^a) (Equation 8),

$$\frac{p}{n^a(p^o - p)} = \frac{1}{n_m^a C} + \frac{(C-1)}{n_m^a C}\left(\frac{p}{p^o}\right) \quad (7)$$

where n^a is the amount adsorbed at the relative pressure p/p^o, and C is a constant related to the enthalpy of adsorption.[49] In addition to monolayer adsorption, this equation requires a linear relationship between $p/n^a(p^o\text{-}p)$ and p/p^o. Usually, this is restricted to p/p^o values of 0.05-0.30.[50] From the BET monolayer capacity, the specific surface area (a_s) can be calculated using Equation 9,

$$a_s = \frac{A_s}{m} = \frac{n_m^a \cdot L \cdot a_m}{m} \quad (8)$$

where A_s is the surface area, and m is the mass of the adsorbent. A_s is defined as the product of the BET monolayer capacity, the molecular cross-sectional area (a_m), and Avogadro's constant (L).

In this work, the specific surface areas of the activated carbon and functionalized activated carbon samples were measured using a Tristar II Plus surface area and porosity analyzer. The samples were analyzed using N_2 adsorption at 77 K with 50 points monitoring adsorption between 0.0065 p/p^0 and 0.995 p/p^0 and 52 points desorption between 0.995 p/p^0 and 0.104 p/p^0. All surface areas were reported using Brunauer-Emmet-Teller (BET) surface area analysis.

2.1.3 Size Exclusion Chromatography (SEC)

Molecular weight (MW) is an important characteristic when describing polymer samples as it greatly affects the properties of the material, including its flocculation performance. Since polymer MWs do not typically occur as a discrete value, MWs are better represented by a variety of statistical averages to describe the molecular weight distribution (MWD) of the polymer sample. Commonly calculated MW statistical averages include the number average molecular weight (M_n) and the weight average molecular weight (M_w). M_n is the statistical average molecular weight of all the polymer chains in the sample and can be described by Equation 10,

$$M_n = \frac{\sum N_i M_i}{\sum N_i} \quad (9)$$

where M_i is the molecular weight of a chain and N_i is the number of chains of that molecular weight. M_n occurs when there are equal numbers of molecules on either side of

M_n in the molecular weight distribution. Comparatively, M_w is the value at which there are equal masses of molecules on each side of M_w in the distribution and can be described by Equation 11,

$$M_w = \frac{\sum N_i M_i^2}{\sum N_i M_i} \tag{10}$$

Since M_w considers the molecular weight of the chains, the value of M_w is sensitive to the high-molecular weight components. Another important value to describe the MWD of a polymer is the dispersity (Đ), which describes the broadness of a molecular weight distribution of a polymer and is defined by Equation 12,

$$Đ = \frac{M_w}{M_n} \tag{11}$$

A larger dispersity value indicates a broader molecular weight distribution. A monodisperse polymer where all the chains are equal has a dispersity index of 1.[19]

Size exclusion chromatography (SEC) is a powerful and convenient technique used to determine the MWD and Đ of a polymer sample. SEC is also commonly referred to as gel permeation chromatography (GPC) or gel filtration chromatography (GFC). While the separation mechanism behind both techniques occurs by size exclusion, GPC often refers to the separation in organic solvents, while GFC is the separation in aqueous solvents. Separation by size exclusion chromatography occurs when molecules of different sizes in the sample pass through a resin packed in a column. When a polymer is dissolved in a solvent, the molecules coil up on themselves to form a coiled conformation. When analyzed by SEC, these coils behave as “tiny spheres” and separate based on their size (hydrodynamic volume). Since the size of the sphere is dependent on

the MW of the polymer (larger spheres for higher MW), polymers of different MWs will separate according to their size as they pass through the column.[19]

The resin used in SEC is composed of spherical beads containing pores of a specific size distribution. Separation occurs when molecules of different sizes are either included or excluded from the pores within the resin, resulting in different elution volumes (Figure 2.4). Molecules that are larger than the largest pores of the resin cannot

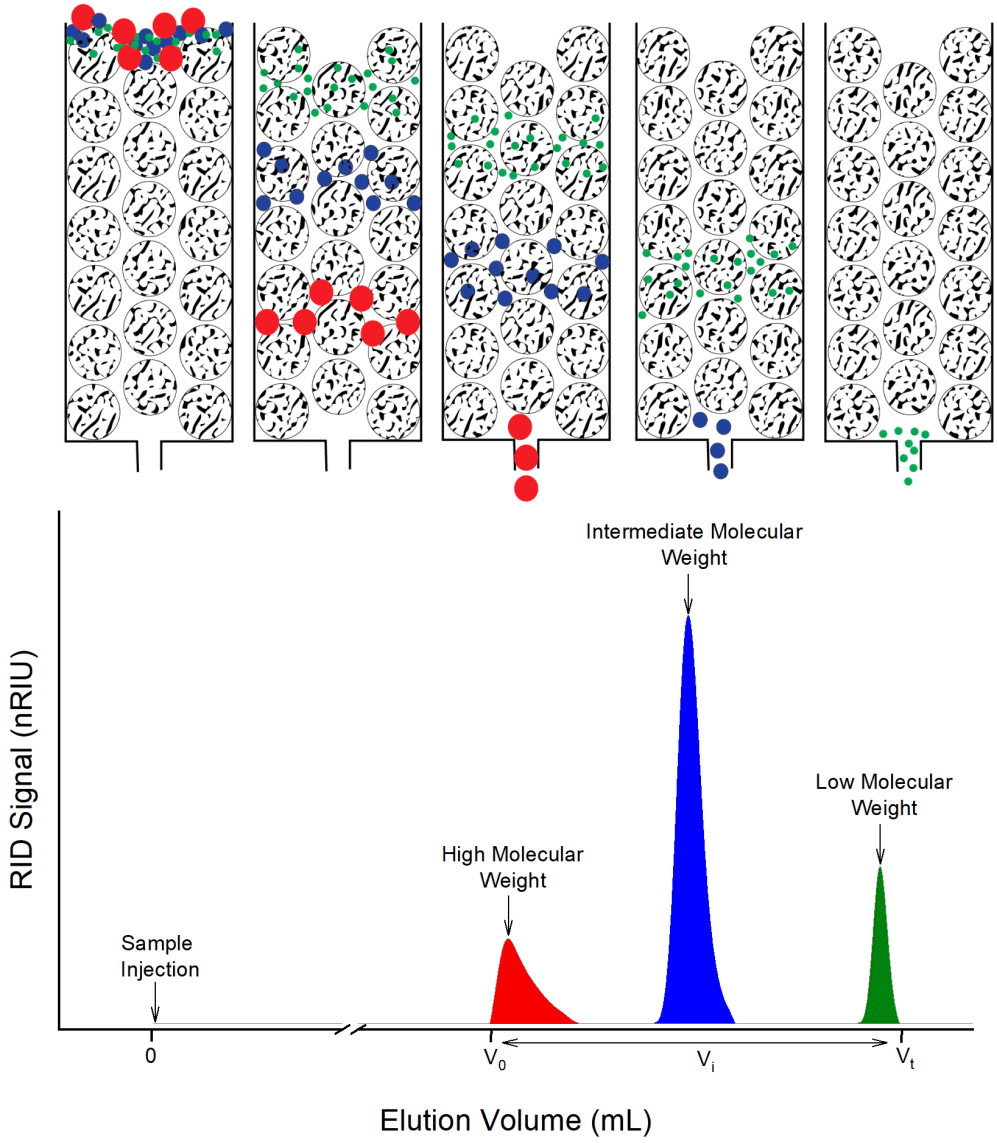

Figure 2.4 *– Illustration of the separation process in size exclusion chromatography and the corresponding chromatogram*

enter the matrix and pass directly through the column, eluting in the void volume (V_0). If the molecules are smaller than the smallest pores in the beads, they have full access to the pores and are not separated as they move down the column. These molecules will elute at the total liquid volume (V_t) which is equal to the void volume plus the total pore volume (V_i). Molecules of intermediate size can enter the larger pores, but not the smaller pores, thereby occupying some of the available stationary phase. These molecules will have an elution volume (V_e) that can be described by Equation 13,

$$V_e = V_0 + K_{SEC}V_i \tag{12}$$

where K_{SEC} is the fraction of the internal pore volume penetrated by those molecules. Since the separation occurs under equilibrium conditions, K_{SEC} can be considered as the equilibrium constant defined by $K_{SEC} = c_i/c_0$, where c_i and c_0 are the concentrations of the molecules inside and outside the pores, respectively. Large molecules that pass directly through the resin without entering the pores will have a K_{SEC} equal to 0, so $V_e = V_0$. Small molecules will have full access to the entire pore volume and will have a K_{SEC} equal to 1, so their $V_e = V_0 + V_i$.[19]

A variety of detectors are available to detect the sample molecules as they elute from the column. In this work, a refractive index detector (RID) was utilized. An RID works by measuring the difference in refractive index between the mobile phase and the pure solvent. The refractive index of a dilute solution (n) is given by Equation 14,

$$n = n_0 + (n' - n_0)c \tag{13}$$

where n_0 is the RI of the solvent, n' is the RI of the sample, and c is concentration of sample in the solution. This can be rearranged to give Equation 15,

$$(n - n_0) = (n' - n_0)c \quad (14)$$

demonstrating that the difference in RI between the solvent and the sample solution is proportional to the sample concentration.[19]

To determine the molecular weight of a polymer sample, the SEC column must be calibrated with standard polymers of known molecule weights (Figure 2.5). Standards need to be of very high quality with extremely narrow molecular weight distributions so that the position of the top of the peak, the peak molecular weight (M_p) can be assigned with confidence. By plotting the log(M_p) vs. elution volume, a calibration curve for the column can be created. From this calibration, the molecular weight distribution of a polymer sample can be calculated. The typical fit functions in SEC are not linear since there is a deviation in linearity close to the exclusion and permeation limits. Therefore, SEC fit functions are typical polynomial functions of higher degree (typically cubic). It should be mentioned that calibration standards should be chemically similar to the analyzed sample molecules. This is because the hydrodynamic volume of a polymer will depend on not only it's MW, but other characteristics such as chemical structure, topology, and the solvent. Since SEC separates molecules according to their hydrodynamic radius, this is important to consider. Polyethylene oxide/polyethylene

glycol standards are commonly used standards for the analysis of aqueous, linear polymers.[19]

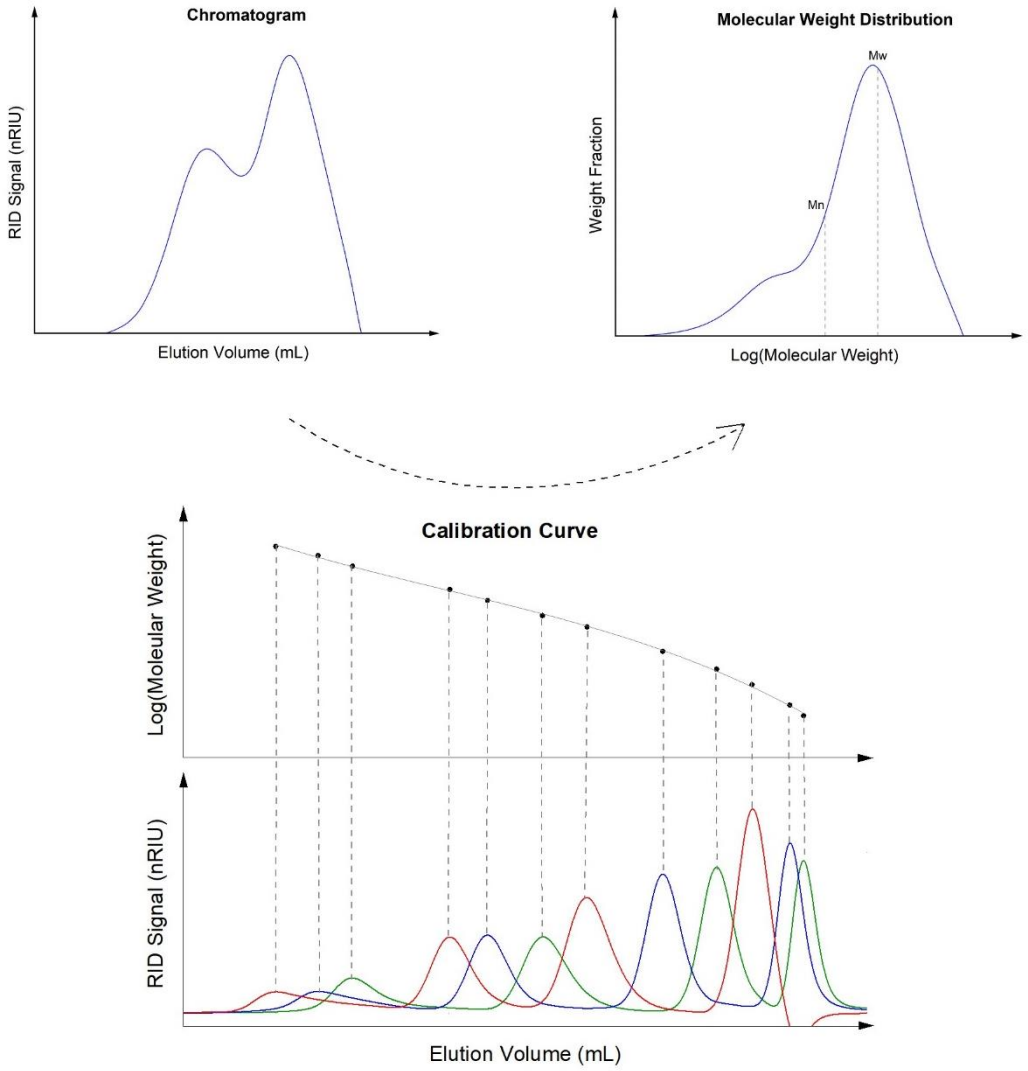

Figure 2.5 *- Converting chromatogram to molecular weight distribution by SEC calibration curve created from a series of standards*

In this work, molecular weights and molecular weight distributions were determined by SEC using Agilent Technologies 1220 Infinity LC equipped with a refractive index detector (RID, Agilent Technologies 1260 Infinity). A PL aquagel-OH MIXED-H 8 μm, 300 x 7.5 mm column was used with an aqueous solution of 0.2 M $NaNO_3$ and 0.01 M NaH_2PO_4 at pH 7 as the mobile phase. Sample concentration and injection volume was 0.20 % (w/v%) and 20 μL, respectively. Chromatography was done at room temperature

with a flow rate of 1 mL/min and the detector was set at 35°C. The column was calibrated with PEO/PEG standard samples with narrow molecular weight distributions in the range of 106 – 1,522,000 g/mol (Agilent Technologies).

2.2 Key Techniques for Measuring Flocculation

2.2.1 Dean-Stark Extraction

Since the flocculation performance of a given flocculant is dependent on the composition of the colloid, it is important to ensure that composition of this colloid is well known and kept consistent throughout the flocculation tests. Additionally, in order to measure the settling behaviour of the suspension, the suspension needs to be diluted so that the polymer can be dispersed throughout the suspension.[51] As the composition of the received MFT sample is variable from batch to batch, Dean-Stark extraction was used to determine the solid, water, and bitumen content of the given sample. A Dean-Stark apparatus consists of a reflux flask, sample & thimble, condenser, and a water trap as shown in Figure 2.6. In a Dean-Stark extraction, the sample (~12.5 g of MFT) is placed in a pre-weighed thimble and hung above a reflux flask containing toluene (~ 200 mL). As the toluene is refluxed, the vapors evaporate the water from the sample, which both rise to the condenser. The immiscible liquids condense and drip into the

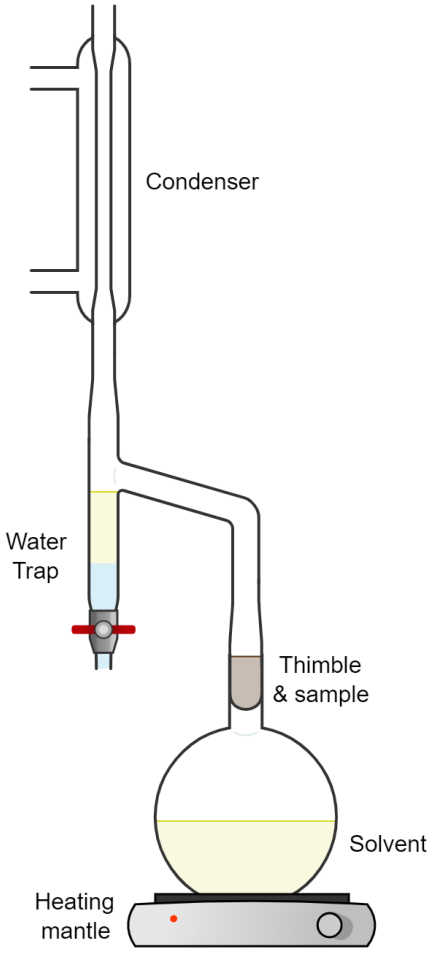

Figure 2.6 *– Illustration of a Dean-Stark apparatus*

trap where they are separated into two layers, with toluene on the top layer. As the toluene in the trap rises to reach the level of the side arm, the toluene drips into the thimble containing the sample. When the toluene flows back into the thimble, the bitumen in the sample is dissolved, which drips back into the flask containing the toluene. The reflux is continued for approximately 24 hours until the solvent dripping from the thimble is visibly free of bitumen. Once the reflux is complete, the thimble is dried in an oven at 110°C overnight and weighed to determine the solid content of the sample. The water from the trap is drained and weighed to determine the moisture content of the sample. Finally, the toluene/bitumen solution is placed in a 250 mL volumetric flask, filled with fresh toluene, and mixed well. 5 mL of the solution was pipetted onto a pre-weighed filter paper and the toluene is allowed to evaporate. Once thoroughly dry, the filter paper is weighed to determine the mass of bitumen in the 5 mL sample. The mass of bitumen in the sample is obtained from the mass of bitumen in 5 mL multiplied by 20.[52]

2.2.2 Settling Tests

Settling tests are performed to measure how quickly a flocculant can settle a given suspension. Settling tests are performed by first mixing the flocculant and suspension at the appropriate dosage, then transferring the suspension

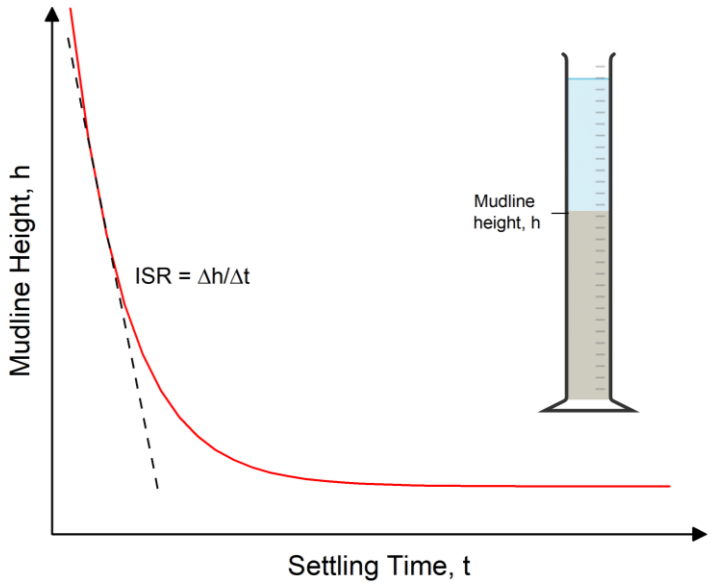

Figure 2.7 *- Settling profile for determination of initial settling rate (ISR)*

to a graduated cylinder to observe the settling. Settling profiles are created by tracking the height of the solid-liquid interface (mudline) as a function of time (Figure 2.7). The initial linear section of the settling profile is often reported as the initial settling rate (ISR), which provides a measurement of the initial flocculation kinetics.[42]

Setting tests were conducted by weighing out 100.0 g of MFT slurry (diluted to 5 wt% solids in deionized water) into a 250 mL beaker. The slurry was mixed at 600 rpm using a three-blade propeller while the flocculant was added. The suspension was mixed at 600 rpm for 2 minutes, followed by 200 rpm for 8 minutes. The mixture was then transferred to a 100 mL graduated cylinder and the change in height of the mudline was recorded over time.[51] A settling profile was obtained by plotting the mudline height vs. time, and the initial settling rate (ISR) was reported as the slope of the initial linear section of the settling profile. After the slurry was allowed to consolidate for 24 hours, the supernatant was carefully pipetted for turbidity measurements.

Measuring the turbidity of a supernatant after flocculation provides information about how effective the flocculant was at settling the fine suspended particles in the MFT sample.[42] In this work, turbidity was measured using a DR/890 Portable Colorimeter (Hach) using an attenuation method. In this method, the intensity of a light beam is measured as it passes directly through a sample. As the light passes through the sample, it will lose intensity due to scattering and absorption. Turbidity units are expressed a Formazin Attenuation Units (FAU).

3. Oxidation of Activated Carbon

3.1 Introduction

Activated carbon (AC) is a porous carbonaceous material produced from the carbonization and activation of raw materials.[1] The highly developed pore structure of ACs give rise to their large surface areas, typically in the range of 800 – 1500 m^2/g.[2] Although the surface of activated carbon is primarily non-polar, the presence of heteroatoms (i.e., oxygen, nitrogen, hydrogen, etc.) can significantly impact the surface chemistry of the material.[5,6] In turn, the surface chemistry of AC affects the properties of the material such as hydrophobicity, surface charge, electronic density of graphene layers, catalytic properties, etc. The concentration of these heteroatoms and functional groups is determined by the nature of the starting material and activation method used to produce the AC, as well as any post-activation surface modifications performed.[7]

Oxygen-containing functional groups are recognized as the most important functional group on the surface of AC as they heavily influence surface chemistry of AC. Oxygen-containing functional groups can be classified as acidic, basic, or neutral (Figure 3.1). Acidic functional groups include carboxyl, lactone, phenol, and anhydrides, while neutral/weakly basic functional groups include carbonyl, quinone, ether, and pyrone.[5] Acidic functional groups are known to increase the hydrophilicity, decrease the point of zero charge, and increase the surface charge density of the activated carbon. These functional groups have been shown to improve the adsorption of metal ion/metallic species from solution by mechanisms of electrostatic attraction, ion exchange, and complex formation.[7] Increasing the content of acidic functional groups also decreases the electronic density of the graphene layers of AC. Since aromatic compounds can adsorb

onto AC through dispersive interactions with those graphene layers, increasing the acidic functional groups content of AC often decreases the adsorption capacity for aromatics.[9]

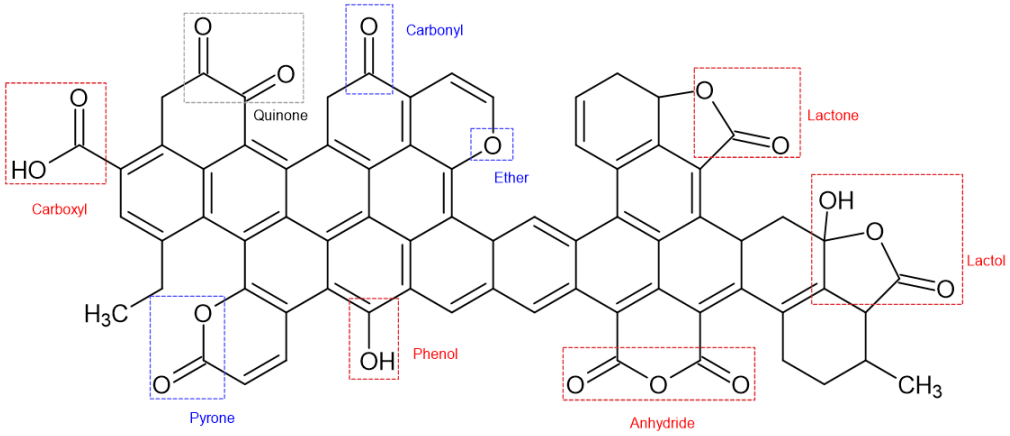

Figure 3.1 *- Potential acidic (red), basic (blue), and neutral (grey) oxygen containing functional groups on the surface of activated carbon*

In addition to altering adsorptive properties, oxygen functional groups can also be used for the grafting of macromolecules onto the surface of activated carbons.[10] For the surface-initiated atom transfer radical polymerization (SI-ATRP) of polymers from activated carbon, an ATRP initiator must first be immobilized onto the surface of activated carbon. Since the density of polymer brushes formed is limited by the density of ATRP initiator on the surface, a high ATRP initiator grafting density should be targeted.[11] However, the surface of activated carbon is relatively unreactive and pre-functionalization is required to provide reactive points on the surface for the grafting of the initiator. The ATRP initiator used in this study, α-bromoisobutyryl bromide, can be grafted onto the surface of AC through the esterification of the acyl bromide groups on the initiator and the oxygen functional groups on the AC (Figure 3.2).[53] In this nucleophilic acyl substitution reaction, hydroxyl/phenol functional groups will yield higher grafting densities than other oxygen functional groups due to their larger nucleophilicity. For this reason, the surface of activated carbon should be pre-

functionalized to increase the oxygen content, specifically in the form of phenol functional groups.

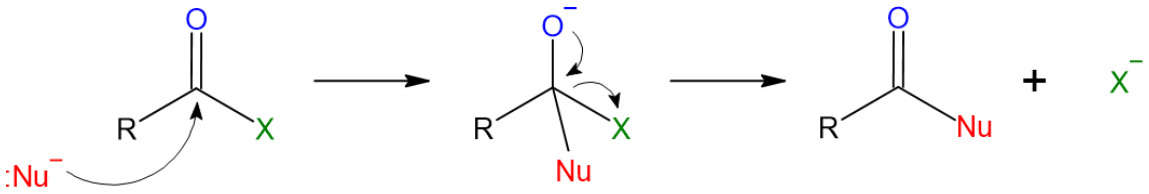

Figure 3.2 – Nucleophilic acyl substitution of acid halides. Occurs by an addition-elimination mechanism where the nucleophile (:Nu) attacks the carbonyl carbon forming a tetrahedral intermediate, followed by the elimination of the leaving group (X)

Oxidation is a commonly used method to tailor the concentration and distribution of oxygen functional groups on the surface of AC.[9] Oxidation methods can be divided into 2 categories – dry and wet oxidation. Dry oxidation involves the utilization of oxidizing gases (i.e., oxygen, ozone, carbon dioxide, etc.) usually at elevated temperatures, while wet oxidation uses oxidizing solutions (i.e., nitric acid, hydrogen peroxide, etc.) under milder conditions.[7] In addition to altering the surface chemistry, oxidation treatments often produce changes in the porous structure of AC, which may also affect its properties. For these reasons, it is important to consider the potential changes in the textural properties of AC when modifying the surface chemistry of the material.[54] Numerous studies have examined the effects of various oxidizing agents on the oxygen content, functional group distribution, and textural characteristics of AC. In a review conducted by Daud and Houshamnd, it was concluded that the information reported in the literature about these effects are inconsistent, and sometimes contradictory.[7] These inconsistencies were attributed to the diversity of oxidation conditions and types of ACs used in the studies reviewed. Oxidation conditions can vary not only by the type of oxidant used, but also by the concentration, temperature, and oxidation time. Activated carbons can also

vary depending on the precursor and activation method used to produce the material, thereby affecting the heteroatom content, surface area, and microporosity content of the AC.[7] All of these factors will influence the chemical and textural changes experienced by an AC after treatment with a given oxidant.

Nitric acid (HNO_3) has been cited as the most used oxidant for AC, likely since the extent of oxidation can easily be controlled by the concentration, temperature, and oxidation time.[54] Most studies report that oxidation by HNO_3 significantly increases the oxygen content of AC, primarily in the form of carboxyl groups. However, oxidation by HNO_3 is also often found to significantly decrease the surface area of AC.[7,9,54,55] Studies on the textural characteristics of ACs produced by oxidation with hydrogen peroxide (H_2O_2) sometimes conflict, where both increases and decreases in surfaces areas have been reported. Similarly, the chemical characteristics sometimes conflict, where some reports indicate an increase in phenol content, while other reports indicate an increase in basic functional groups such as carboxyl, ketone, and ether groups.[7,9,54] Oxidation by ammonium persulfate ($(NH_4)_2S_2O_8$, APS) also has some conflicting reports where both increases and decreases in surfaces areas have been reported. Most studies on the chemical characteristics of ACs treated with APS show an increase in the phenol and carboxyl functional groups, however there is no consensus as to what extent each group increases.[5,7]

Since general conclusions can not be made about the effects of various oxidizing agents, this chapter sets out to find the best oxidizing agent to increase the phenol content of the AC used in our studies. In this chapter, the chemical and textural characteristics of activated carbons treated with HNO_3, H_2O_2, and APS are examined. Additionally, the

effect of oxidation time for these three oxidants was examined, as well as the effect of HNO_3 concentration. The surface chemistry of the various oxidized ACs were evaluated by X-ray photoelectron spectroscopy (XPS), while the textural characteristics were evaluated by N_2 adsorption.

3.2 Materials and Methods

3.2.1 Materials

Potassium hydroxide (KOH), hydrogen peroxide (H_2O_2), nitric acid (HNO_3), ammonium persulfate (APS), and sulfuric acid (H_2SO_4) were purchased from Sigma Aldrich and used as received. Petroleum coke (petcoke) was supplied by Suncor Energy Inc. (Alberta, Canada).

3.2.2 Preparation of Activated Carbon from Petcoke

Approximately 3.0 g of petcoke and 3.0 g of KOH were mixed thoroughly and placed in a stainless-steel crucible. The crucible was placed in an oven under N_2 at 400°C for 30 minutes and removed once cooled to approximately 200-250°C. The sample was well mixed and placed back in an oven under N_2 and heated to 900°C (ramp rate of 60°C/min), then held at 900°C for 15 minutes. The sample was allowed to cool to a minimum of 250°C before removing from the oven. Once cooled to room temperature, the sample was ground with a mortar and pestle, then placed in a beaker with 60 mL of deionized water. The mixture was stirred at 80°C for 1 hour, then vacuum filtered and washed with an additional 60 mL of deionized water at 80°C. The sample was then stirred with 0.1 M HCl (10 mL/g AC) at 80°C for 1 hour, then recovered by vacuum filtration. The resulting activated carbon (AC) was dried in an oven at 110°C overnight.

3.2.3 Oxidation by Nitric Acid

Approximately 1 g of activated carbon was added to a round bottom flask with 10 mL of nitric acid (15.8 M, 10.0 M, and 5.0 M). The mixture was refluxed for a predetermined amount of time. After either 1, 4 or 8 hours, the mixture was cooled to room temperature and filtered by vacuum filtration. The product was washed with deionized water until the washings were approximately neutral. The oxidized AC was dried in a vacuum oven overnight at 110°C. [56]

3.2.4 Oxidation by Hydrogen Peroxide

Approximately 1 g of activated carbon was added to 10 mL of hydrogen peroxide (9.8 M) and stirred at room temperature. After either 1, 4 or 8 hours, the product was collected by vacuum filtration. The product was washed with deionized water until the washings were approximately neutral, then dried in a vacuum oven overnight at 110°C.[56]

3.2.5 Oxidation by Ammonium Persulfate

Approximately 1 g of activated carbon was added to a 15 mL solution of 2.0 M ammonium persulfate in 1.0 M sulfuric acid. The mixture was stirred at 60°C for 1, 4 and 8 hours. The mixture was cooled to room temperature and filtered by vacuum filtration. The product was washed with deionized water until the washings were approximately neutral, then dried in a vacuum oven overnight at 110°C.[5]

3.2.6 Characterization

The specific surface area of the activated carbon and oxidized activated carbon samples were measured using a Tristar II Plus surface area and porosity analyzer. The samples were analyzed using N_2 adsorption at 77 K with 50 points monitoring adsorption between 0.0065 p/p^0 and 0.995 p/p^0 and 52 points desorption between 0.995 p/p^0 and

0.104 p/p^0. All surface areas were reported using Brunauer-Emmet-Teller (BET) surface area analysis. The elemental composition of the activated carbon and oxidized activated carbon samples were measured by X-ray photoelectron spectroscopy (XPS). XPS measurements were performed on a Kratos AXIS supra spectrometer using monochromatic Al K(alpha) source (15mA, 15kV). The instrument work function was calibrated to give a binding energy (BE) of 83.96 eV for the Au 4f7/2 line for metallic gold and the spectrometer dispersion was adjusted to give a BE of 932.6 eV for the Cu 2p3 eV line of metallic copper. The Kratos charge neutralizer system was used on all samples. Survey scan analyses were carried out with an analysis area of 300 x 700 microns and a pass energy of 160 eV. High resolution analyses were carried out with an analysis are of 300 x 700 microns and a pass energy of 20 eV. Analysis of the survey scans and high-resolution scans were performed using CASA XPS (version 2.31), with spectra being corrected to the main line of the C1s spectrum at 284.8 eV. Baseline corrections were made using a Shirley type background correction.

3.3 Results and Discussion

3.3.1 Surface Area by BET

The specific surface area of the oxidized activated carbons was measured and compared to unmodified activiated carbon to evaluate the textural changes imparted by the various oxidiation methods (Figure 3.3). In general, a reduction in surface area of the AC was observed for the various oxidation treatments. It is believed that this is the result of the erosion or destruction of the micropore walls of AC, thereby converting the micropores to mesopores. Additionally, it has been postulated that pore blockage by oxygen surface groups or byproducts of the oxidation can contribute to this apparent

surface area loss.[7] Depending on the oxidant type and severity of the oxidant, the extent of this surface area reduction is varied. The severity of specific oxidant can be controlled by factors such as concentration and oxidation time.

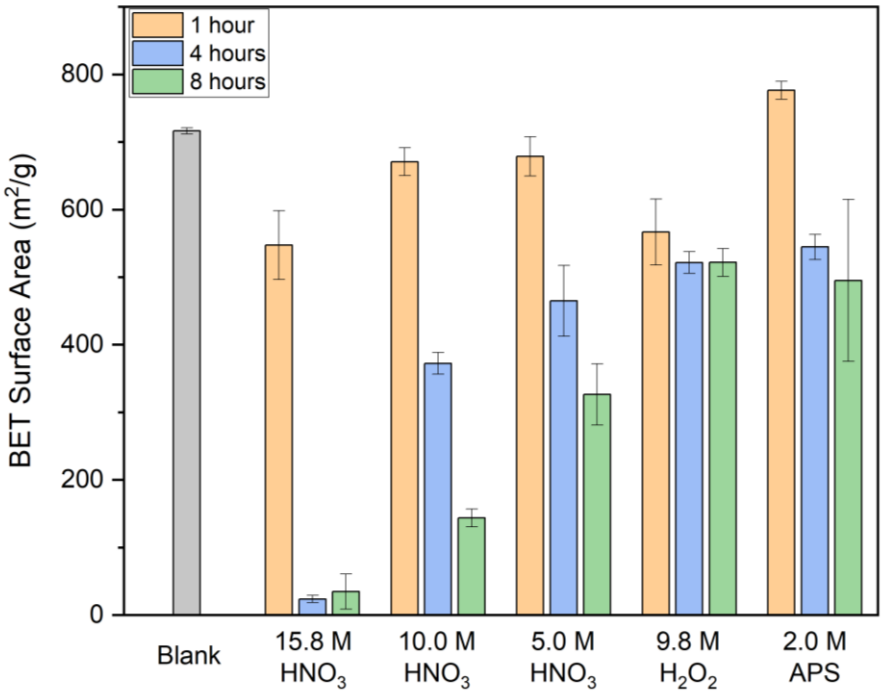

Figure 3.3 *– BET surface areas of unmodified AC and AC oxidized by 15.8 M HNO_3, 10.0 M HNO_3, 5.0 M HNO_3, 9.8 M H_2O_2, and 2.0 M APS for 1 hour, 4 hours, and 8 hours*

Oxidiation by nitric acid was explored at three different concentrations; 5.0 M, 10.0 M, and 15.8 M. At a concentration of 15.8 M, nitric acid reduced the surface area of AC from 716 m^2/g to 547 m^2/g after just 1 hour. For oxidation times of 4 and 8 hours, the surface area was greatly reduced to 24 m^2/g and 35 m^2/g, respectively. As expected, longer oxidation times generally resulted in a greater loss of surface area due to extended exposure time to the oxidant. A similar trend was observed for nitric acid concentrations of 5.0 M and 10.0 M, but to a lesser extent. As expected, lower concentrations of nitric acid resulted in less severe surface area loses. However, for all concentrations of nitric acid investigated, the surface areas of the ACs treated for 4 or 8 hours were still

significantly reduced. Therefore, if nitric acid were to be the oxidant of choice, an oxidation time of 1 hour should be selected.

Compared to oxidiation by nitric acid, oxidiation by hydrogen peroxide had a moderate effect on the surface area of the AC. After 1 hour of oxidiation, the BET surface area of the oxidized AC was reduced to 567 m^2/g. After 4 hours, the surface area was slighly reduced to 522 m^2/g. After 8 hours, the surface area was not significantly changed, potentially indicating that the oxidant is fully consumed after 4 hours.

Finally, oxidiation by ammonium persulfate was shown to have the mildest effect on the surface area of the AC. In fact, the BET surface area of the AC after 1 hour of oxidation was slightly increase to 776 m^2/g. This increase in surface area is suspected to be a result of the removal of the inorganic content of the AC during the oxidation treatment. This demineriliz ation process is further discussed below when evalutating the surface composition of the AC by XPS. After oxidation with APS for 4 and 8 hours, the surface area was reduced to 545 m^2/g and 495 m^2/g, respectively.

3.3.2 Surface composition by XPS

XPS was utilized to evaluate the chemical composition of the unmodified activated carbon and the oxidized activated carbon samples. From the XPS survey scans (Supplementary Material, Figure S1), the elemental composition of the various samples could be quantified (Table 3.1). The unmodified activated carbon was measured to contain a relatively high content of oxygen of 23.46 At%. However, this sample was found to contain a significant portion of several other elements including Si, S, K, Fe, Al, and Ti. Since a large portion of the oxygen in this sample is present as complexes with these other elements, the total oxygen content in this case is not representative of the

carbon-oxygen functional group content of the sample. Depending on the oxidant used, these other elements are removed from the sample during the treatment, which can result in an apparent decrease in the total oxygen content of the sample. This is observed in the APS oxidized samples where the total oxygen content of the samples is reduced after the oxidation treatment. However, the APS oxidation was also found to remove most of the other elements present in the unmodified sample, thereby reducing the At% oxygen in the sample. Comparatively, oxidation by HNO_3 was found to generally increase the total oxygen content of the samples. However, these samples were also found to contain large amounts of Si, contributing to the total oxygen content of the sample.

Table 3.1*- Elemental composition of unmodified AC and oxidized ACs determined from XPS survey scans*

Conditions		**Elemental composition (At %)**					
Treatment	**Time (hrs)**	**C**	**O**	**N**	**Si**	**S**	**Other**
Blank	/	66.50	23.46	0.44	1.67	1.96	K(3.92), Fe(0.62), Ti(0.63), Al(0.80)
15.8 M HNO_3	1	71.58	24.63	1.40	2.27	0.12	
	4	68.46	27.05	1.52	2.76	0.21	
	8	68.53	27.76	0.76	2.85	0.10	
10.0 M HNO_3	1	77.15	21.20	1.32	0.15	0.18	
	4	70.08	25.79	0.84	3.15	0.14	
	8	68.81	27.03	0.72	3.44		
5.0 M HNO_3	1	78.30	20.16	0.69	0.54	0.31	
	4	67.71	26.51	0.53	5.26		
	8	69.31	26.21	1.08	3.41		
9.8 M H_2O_2	1	74.01	23.74	0.40	0.86	0.25	K(0.73)
	4	74.54	23.75	0.23	0.82	0.24	K(0.43)
	8	74.57	23.82	0.36	0.67	0.28	K(0.30)
2.0 M APS	1	79.60	17.61	2.03	0.36	0.41	
	4	77.66	20.39	1.09	0.29	0.57	
	8	77.50	20.62	1.14	0.37	0.37	

Therefore, to determine the effect of the oxidation treatment on the carbon-oxygen functional group content of AC, the speciation of the oxygen in the sample should be considered. The speciation of the oxygen functional groups was determined from the synthetic component fitting of the high-resolution C1s spectra (Figure 3.4).

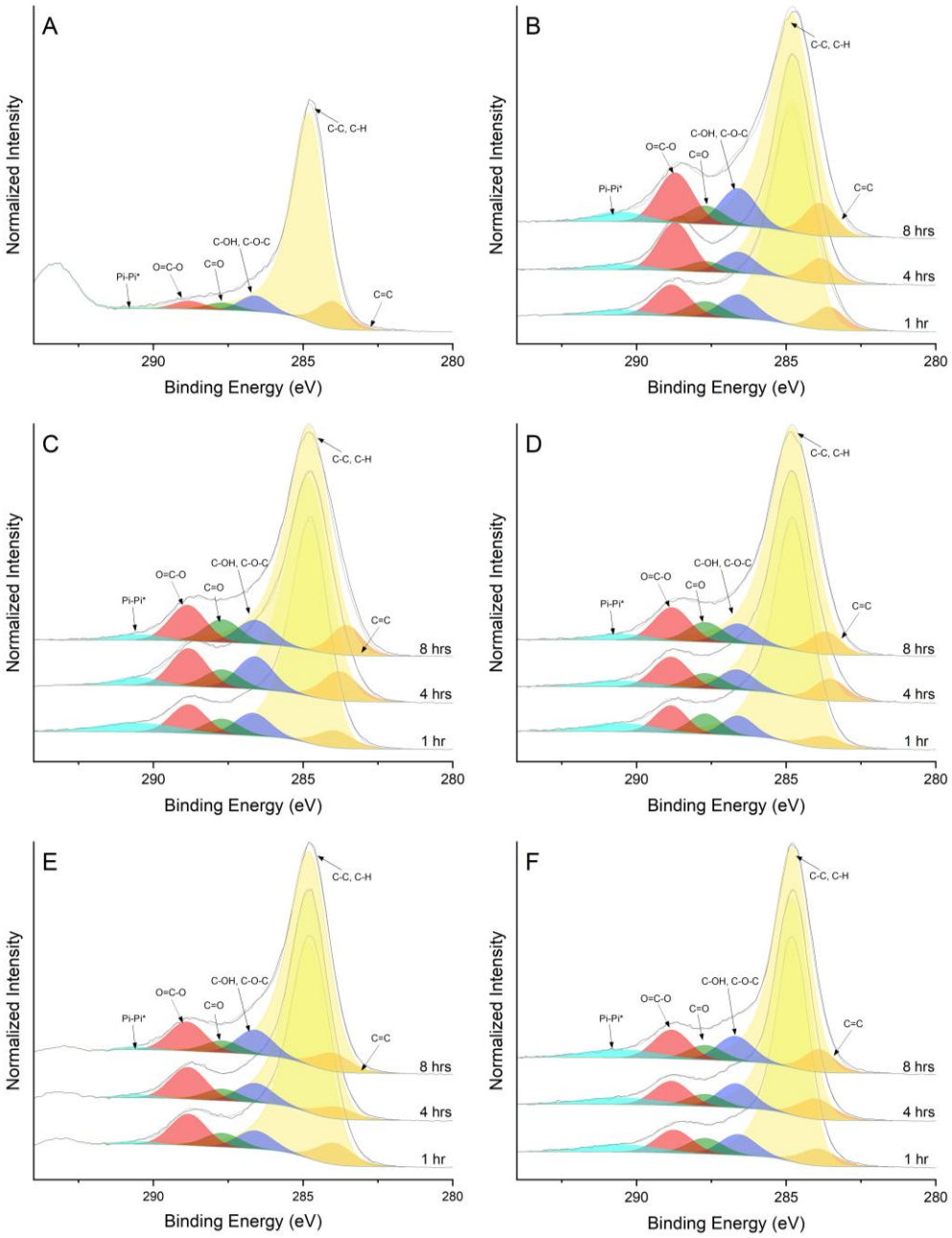

Figure 3.4 *– High resolution C 1s XPS spectra fit with synthetic components of A) unmodified AC, B) 15.8 M HNO_3 oxidized AC, C) 10.0 M HNO_3 oxidized AC, D) 5.0 M HNO_3 oxidized AC, E) 9.8 M H_2O_2 oxidized AC, F) 2.0 M APS oxidized AC*

The high-resolution C1s peak was fit with 6 synthetic components, including two peaks for C-C/C-H species, where sp^2 species are centered at 283.5 – 284.0 eV and sp^3 species are centered at 284.8 – 285.0 eV. Three components were used to fit the oxygenated carbon species, including C-OH/C-O-C (286.4 – 286.7 eV), C=O (287.7 – 288.2 eV), and O=C-O (288.8 – 289.2 eV). An additional broad peak assigned as a pi-pi* transition peak was fit from 290.5 – 292.9 eV. From the percent area of the synthetic component and the atomic percent (At%) of carbon in the sample, the At% of carbon present as the various functional groups could be calculated (Table 3.2).

Table 3.2 *- Results from the synthetic component fitting of the high-resolution C 1s scan of unmodified AC and oxidized ACs. Results are reported as %Area of C1s peak and the calculated atomic percent of carbon present as these species.*

Conditions		**%Area of C1s oxygen components**			**At% C as oxygen components**		
Treatment	**Time (hrs)**	**C-OH, C-O-C**	**C=O**	**O=C-O**	**C-OH, C-OC**	**C=O**	**O=C-O**
Blank	/	5.49	2.54	2.88	3.65	1.69	1.92
15.8 M HNO_3	1	7.29	4.83	9.63	5.22	3.46	6.89
	4	6.18	3.10	14.04	4.23	2.12	9.61
	8	9.31	4.60	12.51	6.38	3.15	8.57
10.0 M HNO_3	1	6.85	4.70	8.66	5.28	3.63	6.68
	4	8.59	4.74	9.99	6.02	3.32	7.00
	8	6.30	6.10	9.59	4.34	4.20	6.60
5.0 M HNO_3	1	5.47	5.68	7.58	4.28	4.45	5.94
	4	5.91	4.51	8.99	4.00	3.05	6.09
	8	5.44	5.53	9.33	3.77	3.83	6.47
9.8 M H_2O_2	1	5.71	4.41	9.94	4.23	3.26	7.36
	4	6.40	3.91	10.6	4.77	2.91	7.90
	8	7.89	3.83	9.35	5.88	2.86	6.97
2.0 M APS	1	7.26	5.52	8.05	5.78	4.39	6.41
	4	8.16	4.17	8.25	6.34	3.24	6.41
	8	7.92	4.64	9.19	6.14	3.60	7.12

Fitting of the high-resolution C 1s illustrated the low carbon-oxygen functional group content of the original unmodified AC. Upon oxidation, the % area of the carbon-oxygen

components C-OH/C-O-C, C=O, and O=C-O increased to varying extents, depending on the oxidation conditions used. At all concentrations investigated, oxidation by HNO_3 resulted in a larger increase of the O=C-O components. In general, larger concentrations of HNO_3 and longer oxidation times resulted in a more significant increase in the oxygen content, especially in the form of carboxylic groups. These results are in agreement with the literature where most reports indicate an increase in the carboxylic acid content upon oxidation with nitric acid. Oxidation by H_2O_2 was also found to primarily increase the concentration of the O=C-O in the sample. Similar to the trend observed in the BET results, increased oxidation times did not have a drastic effect on the oxygen content and distribution in the sample. Finally, oxidation by APS was found to increase both the C-OH/C-O-C and O=C-O components in the sample. Compared to the other oxidation methods, APS produced the largest increase in the C-OH/C-O-C components.

3.4 Conclusions

In this chapter, a variety of oxidation methods were explored to increase the oxygen content of AC, preferentially in the form of phenol functional groups. Three different oxidants were examined, including HNO_3, H_2O_2, and APS. Additionally, the effect of oxidation time for these three oxidants was examined, as well as the effect of HNO_3 concentration. The surface chemistry of the various oxidized ACs were evaluated by X-ray photoelectron spectroscopy (XPS), while the textural characteristics were evaluated by N_2 adsorption. Results from this study showed that oxidation by HNO_3 produced ACs with a higher content of carboxylic acid functional groups. Additionally, oxidation by HNO_3 caused significant surface area loses, especially with higher concentrations of HNO_3 and treatment times exceeding 1 hour. Oxidation by H_2O_2 also produced ACs with

a higher content of carboxylic acid functional groups. Moderate changes in the surface area were observed with the H_2O_2 oxidized AC, where most of the surface area loss occurs in the 1st hour. Oxidation by APS was found to have the mildest effects on surface area of the AC. Additionally, oxidation by APS increased both the C-OH/C-O-C and O=C-O components in the sample. Compared to the other oxidation methods, APS produced the largest increase in the C-OH/C-O-C components. The ideal oxidation time for APS was determined to be 4 hours since this sample had a large surface area and a significant portion of C-OH/C-O-C functional groups. Since phenol groups will be preferentially used during the grafting of the ATRP initiator, APS was chosen as the oxidant for the pre-functionalization of AC in the next chapter.

4. Surface Initiated Polymerization from Activated Carbon

4.1 Introduction

Surface modification techniques such as polymer grafting have the potential to modify the chemical and physical properties of a substrate. Depending on the nature of the grafted polymer, properties of the substrate such as surface wettability, electronic properties, colloidal stability, adsorption capacities, thermal stability, etc., can be altered.[11–14] Due to the repeated chain structure, polymer brushes can impart a high degree of functionality on the surface in which they are grafted. A variety of substrates have been used for polymer grafting, including graphene, carbon nanotubes, metals, metal oxides, proteins, etc.[13–16] However, polymer grafting using activated carbon (AC) as a substrate has rarely been reported. Activated carbon is a carbonaceous material with large surface areas, giving the potential for a high degree of functionalization.[10] Depending on the functional groups present on the grafted polymer, the AC-polymer hybrid could be used for a variety of environmental applications.

Polymer modification of AC utilizing a *grafting through* approach has been reported by a research group in which they synthesized various "covalent organic polymer" functionalized ACs.[28–31] In this approach, the surface of AC was pre-functionalized by oxidation, followed by acyl chlorination. Melamine monomers were then grafted to the surface of AC, providing potential sites for the polycondensation of other monomer units. These covalent organic polymer functionalized ACs were explored for a variety of environmental applications including heavy metal adsorption, organic contaminant adsorption, and impregnation with reactive iron for contaminant degradation.[28–31] However, as is often the issue with the grafting through procedures, control over the

polymer grafting density, molecular weight, and architecture is limited. Additionally, grafting through procedures often require vigorous washing steps to remove the non-grafted polymer also formed during polymerization. Alternatively, a *grafting from* approach for the polymer modification of AC was first developed by Liu and Wang, where surface-initiated atom transfer radical polymerization (SI-ATRP) was used to grow poly(hydroxylethyl acrylate) brushes from the surface of AC.[32] In this approach, the surface of activated carbon was pre-functionalized by oxidation to provide reactive points on the surface for initiator attachment. The surface was then functionalized with an ATRP initiator to form a macroinitiator from which polymerization by ATRP could be performed. Utilizing this approach, AC was modified with a temperature responsive polymer, poly(*N*-isopropylacrylamide) (PNIPAM), to create a self-flocculating AC with response to temperature change.[33,34] This material was designed to remove contaminants from solution when below the lower critical solution temperature (LCST) of PNIPAM, as well agglomerate when the temperature is above the LCST. This self-flocculating effect allowed the AC-PNIPAM to be easily retrieved from solution after treatment, thereby eliminating potential secondary pollution and allow for the potential of recycling the AC-PNIPAM.[33,34]

An advantage to the SI-ATRP method is the opportunity to control polymer brush thickness, composition, and architecture. The synthesis of polymers using reversible-deactivation radical polymerization (RDRP) techniques such as ATRP should display pre-determinable degrees of polymerization, low dispersity, first-order kinetics, and long-lived polymer chains with preserved end-functionalities.[18] In ATRP, this is achieved by establishing a dynamic activation/deactivation equilibrium between propagating radicals

and dormant alkyl halide species. The dormant species can be activated by reacting with a transition metal catalyst in its lower oxidation state to form the propagating radicals.[24] However, due to the low oxidative stability of these complexes, careful handling techniques are required. Additionally, the reaction mixture must be carefully deoxygenated using techniques such as the freeze-pump thaw degassing process.[25] This is particularly difficult in aqueous polymerization solutions, resulting in poor control over the polymerization.[26] This issue can be overcome by using a catalyst in its higher oxidation state in addition to a chemical reducing agent, such as ascorbic acid, to generate the lower oxidation state catalyst in situ.[25] In this process, named activators generated by electron transfer (AGET) ATRP, the oxygen sensitivity of the reaction is reduced by using a more oxidatively stable transition metal complex and through the reduction of any oxygen in the reaction flask. Utilizing this approach, Liu et. al. reported the grafting of methyl methacrylate and *tert*-butyl acrylate from the surface of AC.[36] By employing AGET ATRP in place of ATRP, the oxygen sensitivity of the reaction is reduced, as well, a lower concentration of metal catalyst can be used.[25]

In this chapter, the polymer polyacrylamide (PAM) was grafted from the surface of activated carbon utilizing SI-AGET ATRP (Figure 4.1). This material was designed to explore the use of a polymer modified AC for the flocculation and dewatering of mature fine tailings (MFT). While this chapter focuses on the synthesis and characterization of polyacrylamide grafted activated carbon, *Chapter 5* will explore the flocculation performance of the material.

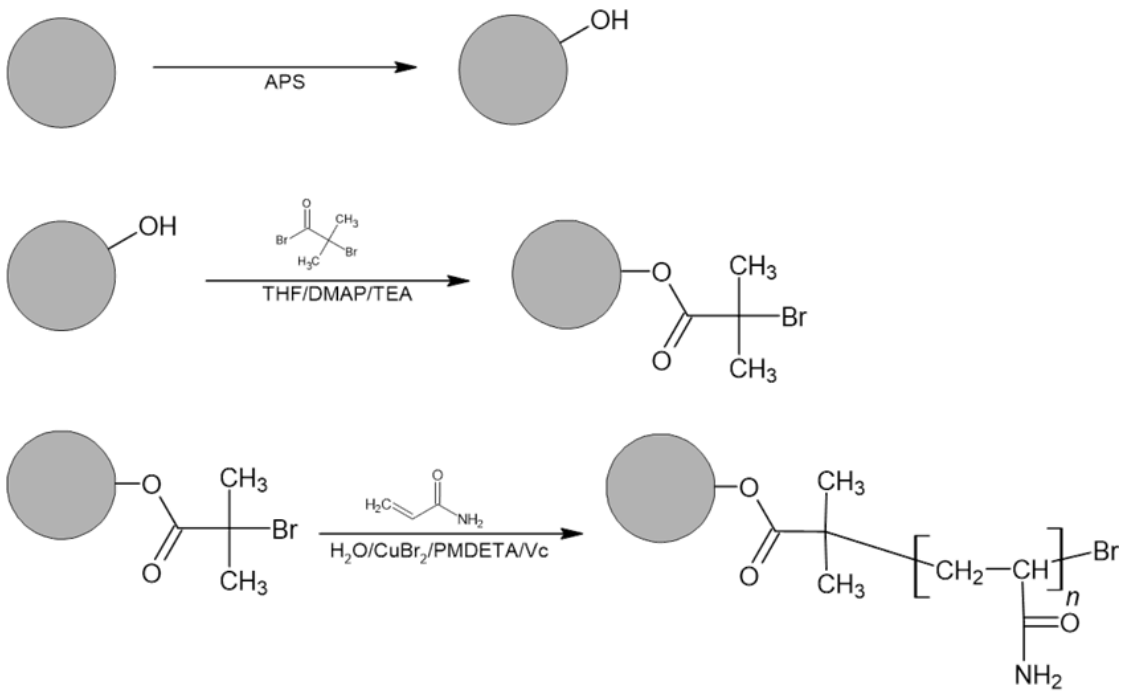

Figure 4.1 *- Synthesis scheme for preparation of polyacrylamide modified AC*

4.2 Materials and Methods

4.2.1 Materials

4-dimethylaminopyridine (DMAP), α-bromoisobutyryl bromide (BiBB), tetrahydrofuran (THF), and methanol were purchased from Sigma Aldrich and used as received. Acrylamide (AM, Thermo Scientific), N,N,N',N",N"-pentamethyldiethylenetriamine (PMDETA,TGI America), ascorbic acid (AscA, Bio Basic), acetone (Fisher Chemicals), and $CuBr_2$ (Alfa Aesar) were used as received. Triethylamine (TEA) was purchased from Alfa Aesar and was dried 4 Å molecular sieves before use.

4.2.2 Preparation of AC

Activated carbon (AC) was prepared from petroleum coke, as described in *Chapter 3.2.2.*

4.2.3 Preparation of oxidized AC (AC-OH)

Activated carbon was oxidized using ammonium persulfate (AC-OH), as described in *Chapter 3.2.5.*

4.2.4 Preparation of initiator grafted AC (AC-BiBB)

2.46 g of AC-OH, 0.147 g of DMAP (1.20 mmol), 50 mL of THF, and 2.8 mL of TEA (20 mmol) were added to a 100 mL round bottom flask. The mixture was dispersed in an ultrasonic bath for 30 minutes, then transferred to an ice-salt bath and placed under N_2. Once cooled, 1.075 mL of BiBB (8.7 mmol) in 13 mL of THF was added to the flask dropwise. The mixture was stirred on ice for 3 hours, then at room temperature for a total of 48 hours. The mixture was filtered and washed with acetone, then washed with deionized water. The resulting product was dried in a vacuum oven at 40°C and denoted as AC-BiBB.[36]

4.2.5 Surface-initiated AGET ATRP of acrylamide from AC-BiBB (AC-PAM)

0.1035 g of AC-BiBB, 10.662 g of acrylamide (0.15 mols), and 49 mL of Millipore water were added to a round bottom flask and purged with N_2 for 30 minutes. 0.5 mL of an aqueous catalyst solution containing $CuBr_2$ ($1.5x10^{-5}$ mol) and PMDETA ($1.5x10^{-4}$ mol) was injected into the flask and sealed under N_2. The solution was heated to 60°C and 0.5 mL of an aqueous solution containing ascorbic acid ($1.5x10^{-4}$ mol) was injected to initiate polymerization.[36] After 24 hours, the solution was cooled and centrifuged at 8700 rpm to collect the product. The supernatant was discarded, and the product was re-dispersed in water and centrifuged again at 8700 rpm. This process was repeated 3 times to remove any free or physically absorbed polymer. The resultant product denoted AC-PAM was collected and dried in a vacuum oven at 40°C.

4.2.6 Hydrolysis of PAM from AC-PAM

To measure the molecular weight of the grafted polymer, the polymer was first cleaved from the surface of AC by acid catalyzed hydrolysis (Figure 4.2). This was accomplished by refluxing 0.5 g of AC-PAM with 25 mL of Millipore water and 0.25 mL of concentrated HCl at 100°C for 3 hours. After the reflux was complete, the solution was cooled to room temperature and vacuum filtered to remove the AC. The filtrate was precipitated in excess methanol and vacuum filtered to recover the cleaved polymer. The cleaved polymer was dried in an oven at 40°C overnight.[57]

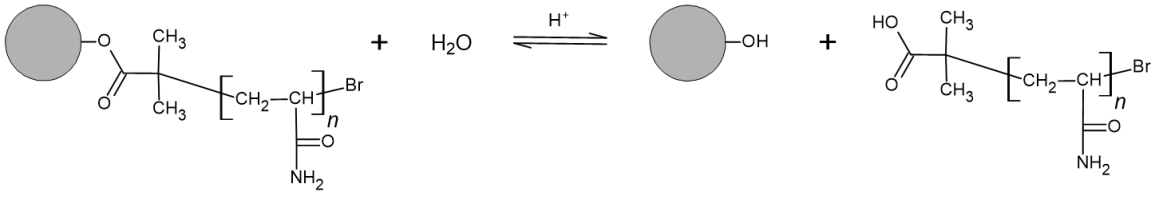

Figure 4.2 *- Acid catalyzed hydrolysis of PAM from AC-PAM*

4.2.7 AGET ATRP of acrylamide (PAM)

Acrylamide was polymerized by AGET ATRP using the same polymerization conditions as the SI-AGET ATRP of acrylamide. Instead of growing the polymer from the surface of AC-BiBB, the polymer was synthesized using BiBB as the initiator. For this synthesis, 10.662 g of acrylamide (0.15 mols) and 49 mL of Millipore water was added to a round bottom flask and purged with N_2 for 30 minutes. 0.5 mL of an aqueous catalyst solution containing $CuBr_2$ ($1.5x10^{-5}$ mol) and PMDETA ($1.5x10^{-4}$ mo)l was injected into the flask and sealed under N_2. The solution was heated to 60°C and 3.72 μL of BiBB ($3.0x10^{-5}$ mols) was added to the flask. 0.5 mL of an aqueous solution containing ascorbic acid ($1.5x10^{-4}$ mol) was injected to initiate polymerization. After a pre-determined amount of time, an aliquot was taken from the reaction flask and the

polymer was precipitated in methanol. The polymer was recovered by vacuum filtration, washed with methanol, and dried in a vacuum oven at 40°C.

4.2.8 Characterization

Fourier transform infrared spectroscopy (FTIR) was employed to determine the functional groups present in the various AC samples. All samples were analyzed using a Nicolet 380 FTIR spectrometer with a diamond crystal attenuated total reflectance (ATR) accessory. Measurements were performed with 128 scans per analysis within the range of 400-4000 cm^{-1}.The elemental composition of the modified activated carbon samples was measured by X-ray photoelectron spectroscopy (XPS), as described in *Chapter 3.2.6.* Specific surface areas were measured using a Tristar II plus surface area and porosity analyzer, as described in *Chapter 3.2.6.* Thermogravimetric analysis (TGA) was performed to determine the weight percent of grafted material on the surface of the modified activated carbon samples. Analyses were performed using a TA instruments Q600 SDT thermal analyzer. The samples were heated at a rate of 10 °C/min from room temperature to 1000 °C under argon with a flow rate of 20 mL/min. The molecular weight and molecular weight distribution of the cleaved polymer was determined by size exclusion chromatography (SEC) using Agilent Technologies 1220 Infinity LC equipped with a refractive index detector (RID, Agilent Technologies 1260 Infinity). A PL aquagel-OH MIXED-H 8 μm, 300 x 7.5 mm column was used with an aqueous solution of 0.2 M $NaNO_3$ and 0.01 M NaH_2PO_4 at pH 7 as the mobile phase. Sample concentration and injection volume was 0.20 % (w/v%) and 20 μL, respectively. Chromatography was done at room temperature with a flow rate of 1 mL/min and the detector was set at 35°C. The column was calibrated with PEO/PEG standard samples

with narrow molecular weight distributions in the range of 106 – 1,522,000 g/mol (Agilent Technologies).

4.3 Results and Discussion

4.3.1 Characterization of AC-PAM

FTIR was utilized to monitor the evolution of the functional groups on the surface of activated carbon throughout the various steps of the modification. As shown in Figure 4.3, the oxidized AC contains a variety of oxygen containing functional groups, evidenced by C=O stretching at 1724 cm^{-1}, C-O stretching at 1209 cm^{-1} and 1162 cm^{-1}, and C-OH stretching at 1037 cm^{-1}. Upon functionalization with the ATRP initiator, a

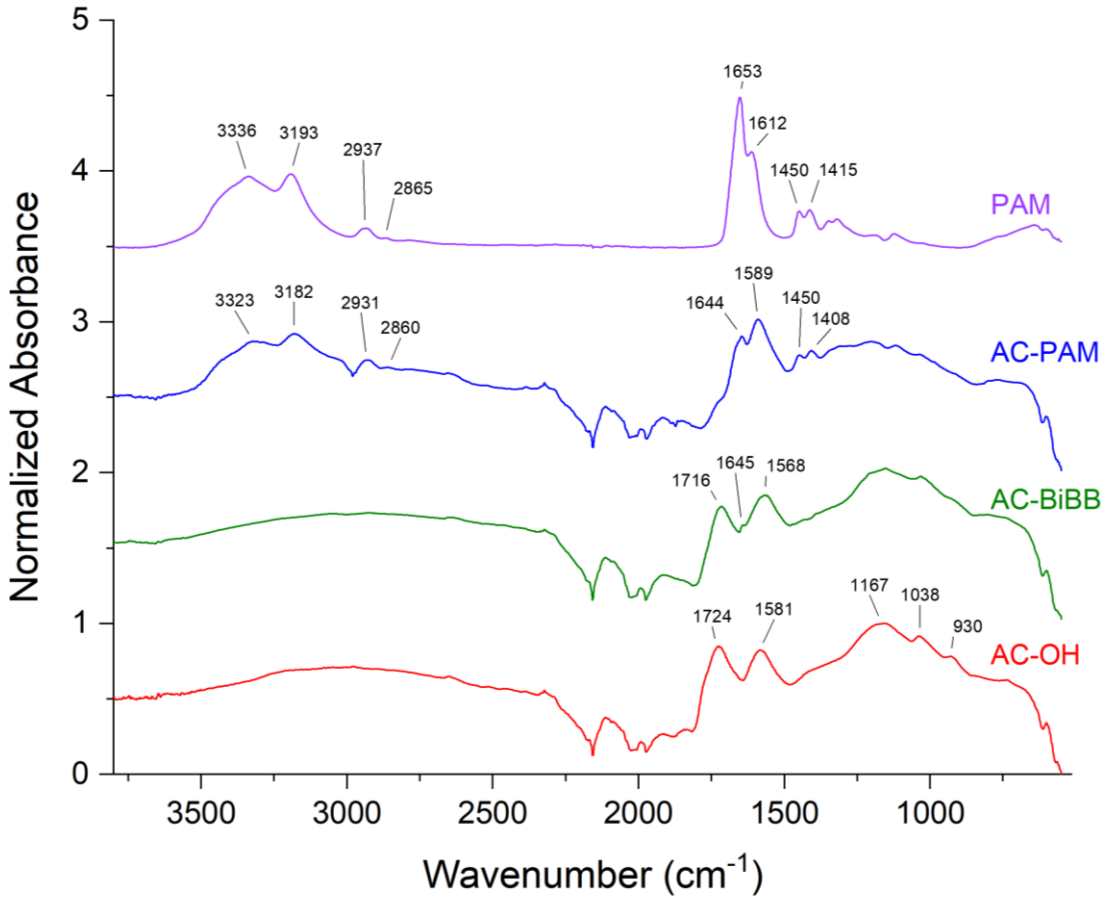

Figure 4.3 *- FTIR of oxidized AC (AC-OH), ATRP initiator modified AC (AC-BiBB), polyacrylamide modified AC (AC-PAM), and polyacrylamide (PAM)*

small additional peak at 1643 cm^{-1} corresponding to the C=O stretching vibration of the initiator is observed. After polymerization, a variety of peaks corresponding to the functional groups of polyacrylamide are observed on the surface of AC. These peaks include NH_2 asymmetric stretching at 3395 cm^{-1}, NH_2 symmetric stretching at 3193 cm^{-1}, sp^3 CH_2 asymmetric stretching at 2937 cm^{-1}, NH_2 bending at 1589 cm^{-1}, sp^3 CH_2 bending at 1450 cm^{-1}, and C-N stretching at 1408 cm^{-1}.

XPS was utilized to determine the elemental composition and speciation of the various modified AC-samples. From the XPS survey scan (Supplementary Material, Figure S2), the elemental composition of the various modified AC-samples was determined (Table 4.1). When comparing the composition of the unmodified AC and the oxidized AC, the oxygen content in the sample drops from 23.46 At % to 20.39 At% upon oxidation. However, since the unmodified AC contains several other elements including Si, S, K, Fe, Al, and Ti, a large portion of the oxygen in this sample is present as complexes with these other elements and not as carbon-oxygen functional groups. During the oxidation process, a significant portion of these complexes are removed from the AC, resulting in a loss of total oxygen in the sample. Although the total oxygen

Table 4.1 *– Elemental composition of unmodified AC, oxidized AC (AC-OH), ATRP initiator functionalized AC (AC-BiBB), polyacrylamide functionalized AC (AC-BiBB), and polyacrylamide (PAM)*

Sample	**Elemental composition (At %)**						
	C	**O**	**N**	**Br**	**Si**	**S**	**Other**
AC	66.50	23.46	0.44	-	1.67	1.96	K (3.92), Fe (0.62), Ti (0.63), Al (0.80)
AC-OH	77.66	20.39	1.09	-	0.29	0.57	-
AC-BiBB	75.47	21.23	1.80	0.16	0.69	-	-
AC-PAM	71.59	17.85	9.87	-	0.65	0.05	-
PAM	63.18	18.15	18.66	-	-	-	-

content in the sample did not increase during oxidation, oxidation did increase the concentration of carbon-oxygen functional groups on the surface of AC.

This can be confirmed when comparing the peak fitting for the high-resolution C 1s scan of the samples (Figure 4.4), which was fit with 6 synthetic components; C=C (283.5 – 284.0 eV), C-C/C-H (284.8 – 285.0 eV), C-OH/C-OC (286.4 – 286.7 eV), C=O (287.7 – 288.2 eV), O=C-O (288.8 – 289.2 eV), and pi-pi* (290.5 – 292.9 eV). After oxidation, there is an increase in the % area of the carbon-oxygen components C-OH/C-O-C, C=O, and O=C-O, indicating successful oxidation (Supplementary Material, Table S2) These carbon-oxygen functional groups served as attachment points for the ATRP initiator.

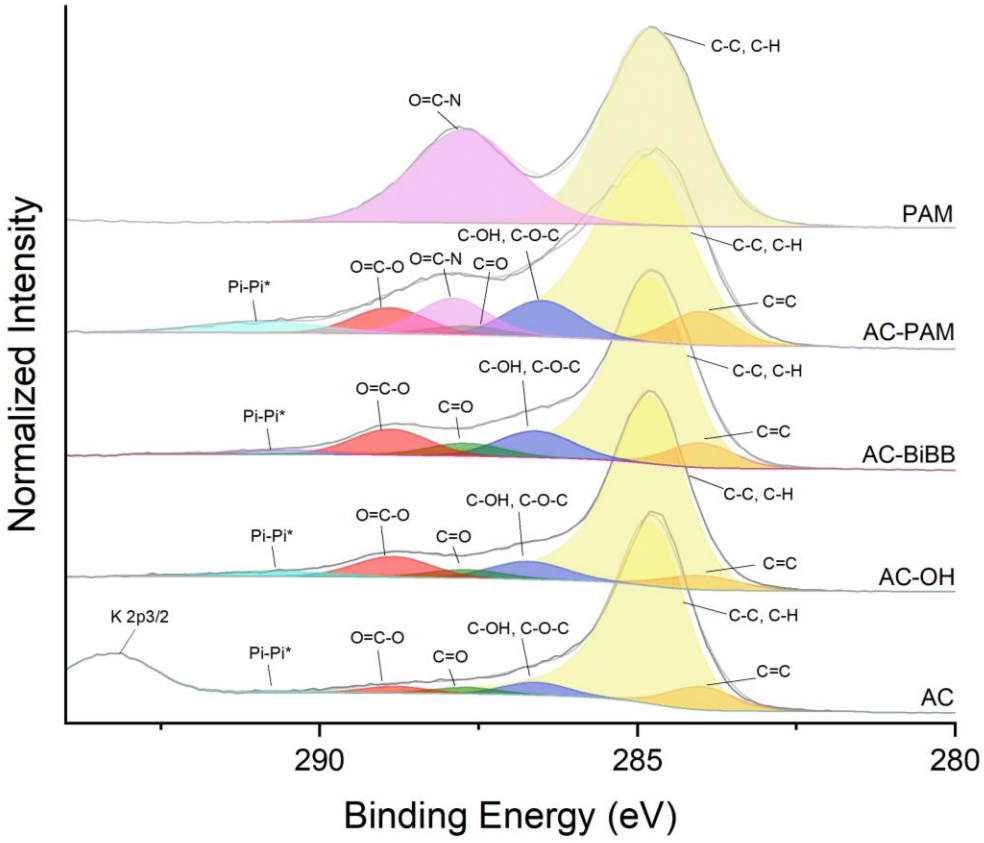

Figure 4.4 *– High-resolution C 1s scans with synthetic components for unmodified activated carbon (AC), oxidized AC (AC-OH), ATRP initiator modified AC (AC-BiBB), polyacrylamide modified AC (AC-PAM), and polyacrylamide (PAM)*

Upon grafting of the ATRP initiator, a small peak corresponding to 0.16 At% Br is measured in the sample. While this represents a relatively small amount of initiator grafted to the surface, this was sufficient for the growth of polymer, evidenced by the large atomic percent of nitrogen in the AC-PAM sample (9.87 At%). The high-resolution N 1s scan of AC-PAM was fit with three synthetic components, including nitrogen present as amides, graphitic nitrogen, and oxidized nitrogen (Figure 4.5).[55] Most of the nitrogen (75%) in the AC-PAM sample is present as amides , indicating the successful grafting of polyacrylamide (Supplementary Material, Table S3). This is further supported by the high-resolution C 1s of AC-PAM, showing the addition a O=C-N component (Figure 4.4). Therefore, the XPS results support the successful grafting of PAM on the surface of AC.

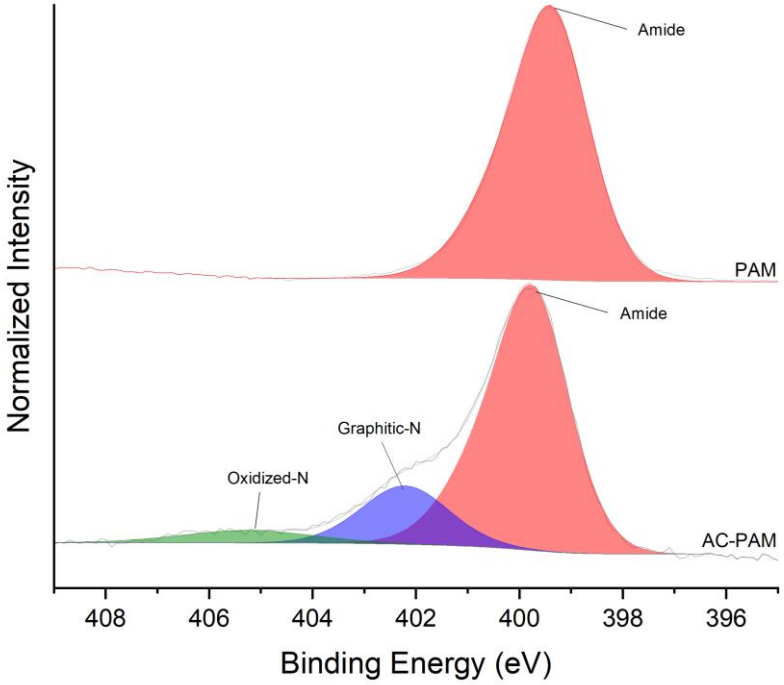

Figure 4.5 *– High-resolution N 1s scans with synthetic components for polyacrylamide modified activated carbon (AC-PAM) and polyacrylamide (PAM)*

Surface areas of the different AC samples were measured by BET. After oxidation, the surface area of the AC decreased from 716 m^2/g to 545 m^2/g. After grafting of the ATRP initiator, the surface area of AC-BiBB is reduced to 240 m^2/g. This reduction in

surface area is due to attachment of the macroinitiator, thereby increasing the non-porous content of the AC as well as potentially blocking the pores of AC. After surface-initiated polymerization, the surface area of the AC-polymer composite is greatly reduced to 7 m^2/g. This is attributed to the inclusion of the non-porous PAM on the surface of AC, as well as the polymer chains potentially blocking the pores of the AC when not extended in solution.[36]

Thermogravimetric analysis (TGA) was used to estimate the amount of grafted material on the surface of the modified activated carbons (Figure 4.6). All samples show an initial weight loss from the evaporation of water in the range of 70-110°C. A second weight loss occurs at approximately 185-290°C and was attributed to the decomposition of oxygen functional groups on the surface of AC, as well as the initiator groups on the surface of AC-BiBB.[36] Comparing the residual masses after heating to 800°C, it was observed that AC-BiBB experienced an additional 4.03 wt% loss in weight when compared to AC-OH. From this, it was estimated that the AC-BiBB sample contains approximately 4.04 % of initiator by weight, corresponding to 0.269 mmol of BiBB/g of AC-BiBB. When comparing the TGA profile of the AC-PAM and PAM, they share similar decomposition profiles with major weight losses in the range of 280-330°C and 390-440°C, corresponding to the decomposition of NH_2 and the decomposition of the polymer backbone, respectively. After heating to 800°C, the residual mass of the AC-PAM was 45.72%, compared to the AC-BiBB which was 56.32%. The increase in weight loss of 10.6% in the AC-PAM was attributed to the decomposition of PAM, indicating that the AC-PAM contains approximately 10.6% PAM by weight.

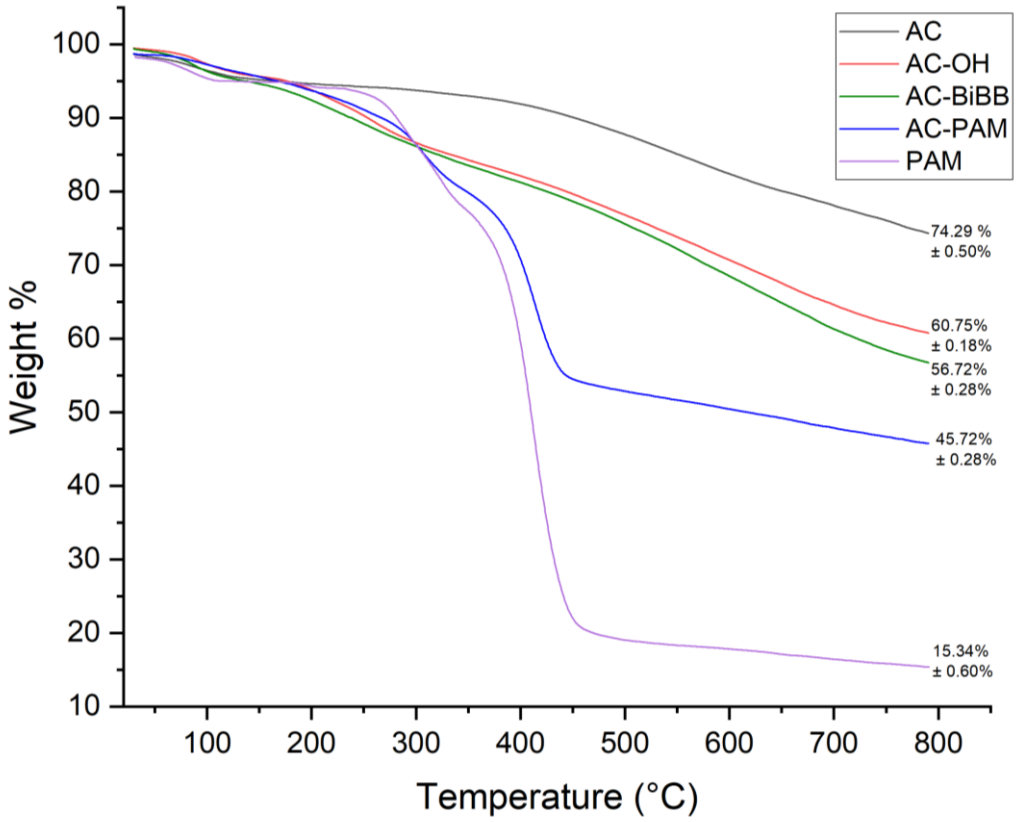

Figure 4.6 *- TGA profile of unmodified AC, oxidized AC (AC-OH), ATRP initiator modified AC (AC-BiBB), polyacrylamide modified AC (AC-PAM), and polyacrylamide (PAM)*

4.3.2 Molecular weight determination

The theoretical molecular weight of a polymer produced by RDRP can be predicted from the degree of polymerization (DP_n) and the molar mass of the monomer units (M_0).[19] The DP_n is defined as the ratio of the concentrations of consumed monomer [M] and initiator initially introduced $[I]_0$ (Equation 16).

$$M_n = DP_n \, x \, M_0 = \frac{\Delta[M]}{[I]_0} x \, M_0 \qquad (15)$$

The concentration of initiator initially introduced in the reaction for the synthesis of AC-PAM was estimated from the concentration of initiator on the surface of AC, as determined by TGA. From this, the monomer to initiator ratio of this polymerization was

estimated as roughly 5000:1, which should produce a polymer with a molecular weight of 355,500 g/mol if 100% monomer conversion is achieved. The molecular weight of the grafted polymer was measure by first cleaving the polymer from the surface of AC using acid catalyzed hydrolysis. The cleaved polymer was then analyzed using size exclusion chromatography and was eluted at a volume of 7.64 mL. Using the calibration curve created by a series of PEO/PEG standards (Supplementary Material, Figure S3), a molecular weight distribution for the cleaved polymer was determined (Figure 4.7). The number-average molecular weight (M_n) of the cleaved polymer was calculated as 176,100 g/mol with a dispersity value of 2.10. When compared to the theoretical molecular weight (assuming 100% monomer conversion), the cleaved polymer has a significantly lower molecular weight. Additionally, the dispersity of the polymer was relatively large for a polymer synthesized by RDRP, where dispersity values are typically in the range of 1.01-1.5.[19,23]

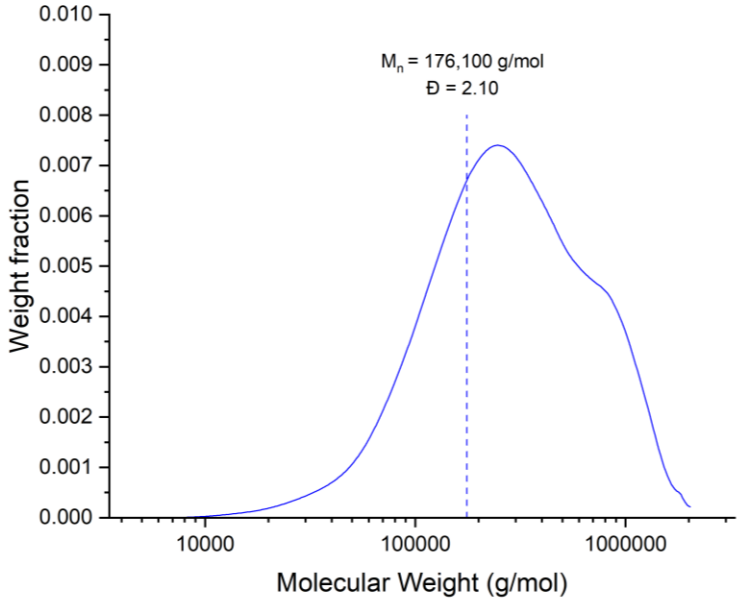

Figure 4.7 *– Molecular weight distribution of cleaved PAM from AC-PAM*

A potential reason for the deviation between the theoretical and measured molecular weights could be from the "chopping up" of the polymer during the acid catalyzed hydrolysis of AC-PAM. To investigate this, the molecular weight of PAM synthesized under the same conditions of AC-PAM was compared to the molecular weight of the

cleaved polymer. PAM was synthesized using α-bromoisobutyryl bromide as the initiator instead of AC-BiBB, with the same monomer to initiator ratio of 5000:1. Similar to the grafted polymer, acrylamide polymerized by AGET ATRP with a monomer to initiator ratio of 5000:1 should produce a polymer with a molecular weight of 355,500 g/mol if 100% monomer conversion is achieved. After polymerization for 24 hours, the number-average molecular weight of PAM was measured as 194,300 g/mol with a dispersity value of 2.56 (Figure 4.8). Since the non-grafted polymer was measured to have similar M_n and dispersity values, it is unlikely that the "chopping up" of the polymer during the hydrolysis of AC-PAM occurs.

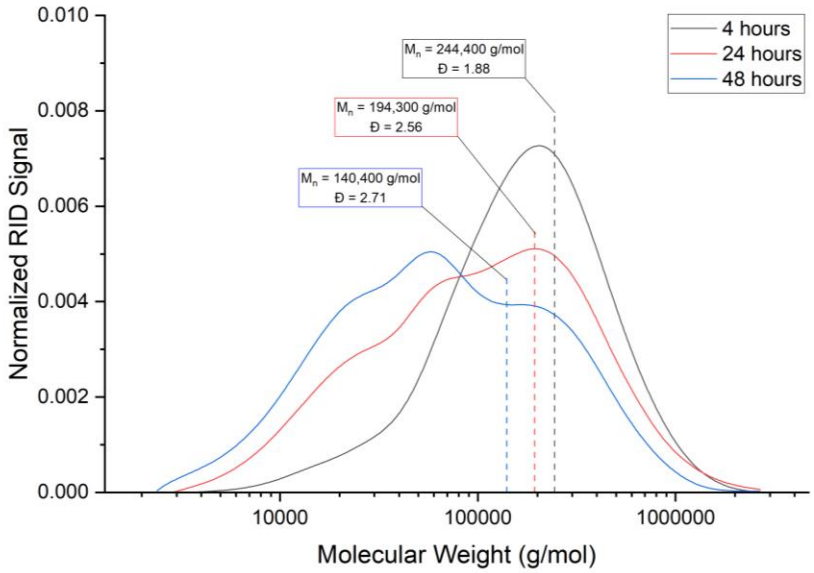

Figure 4.8 *– Normalized RID signal vs. molecular weight of polyacrylamide (PAM) synthesized from AGET ATRP*

An alternative explanation for the low molecular weight and relatively large dispersity values of PAM synthesized by AGET ATRP could be due to suboptimal polymerization conditions. If the polymerization is truly controlled, we should see an increase in molecular weight as the polymerization progresses and monomer is consumed. To probe this, the molecular weight of PAM synthesized using a monomer to initiator ratio of 5000:1 was monitored as a function of polymerization time (Figure 4.8). After polymerization for 4 hours, the M_n of PAM was measured as 244,400 g/mol with a

dispersity of 1.88. However, as polymerization time increased, the M_n of the polymer was found to decrease over time, while the dispersity increased, indicating poor control over the polymerization. In ATRP, control over the polymerization is achieved by establishing a fast activation-deactivation equilibrium between radicals and dormant alkyl halides.[24] The ATRP equilibrium constant (K_{ATRP}) for a reaction is influenced by a variety of factors including the structure of the catalyst and monomer/dormant species. Additionally, reaction conditions such as the solvent, temperature, and pressure can strongly influence the K_{ATRP}.[18,24] If the reaction conditions are not appropriately selected, undesirable reactions such as radical termination may occur.[24] Additionally, slow initiation or the occurrence of irreversible transfer reactions can result in poor control over the polymerization. In order to achieve control over the polymerization of acrylamide by AGET ATRP, a complete investigation of the polymerization conditions could be carried out. If the conditions are appropriately selected, the polymerization should display first-order kinetics and a linear increase in molecular weight with monomer conversion. If control over the polymerization is achieved, PAM could hopefully be synthesized to higher molecular weight.

4.4 Conclusions

In this chapter, polyacrylamide grafted activated carbon was successfully synthesized using surface-initiated AGET ATRP. The presence of grafted polymer on the surface of activated carbon was confirmed by characterization with FTIR and XPS. The FTIR of AC-PAM contained numerous peak corresponding to the stretching and bending vibrations of the functional groups present in polyacrylamide. The XPS results indicated that the AC-PAM sample contains approximately 9.87 At% nitrogen, further supporting

the grafting of polyacrylamide from the surface of AC. The weight percent of grafted polymer was estimated as 10.6 % from the TGA results. The molecular weight of the grafted polymer was measured as 176,100 g/mol with a dispersity value of 2.10. While the characterization results indicated successful grafting of polyacrylamide from the surface of activated carbon, the polymer molecular weight and dispersity values indicate poor control over the polymerization. This was confirmed when investigating the polymerization of acrylamide by AGET ATRP. The following chapter will examine the flocculation performance of AC-PAM and compare this to the flocculation performance of PAM.

5. Flocculation performance of AC-PAM

5.1 Introduction

The Canadian oil sands located in the province of Alberta represent the third largest proven oil reserves in the world, containing an estimated 177 billion barrels of recoverable oil.[37] Depending on the depth of the reserves, bitumen can be extracted from the oil sands utilizing surface mining (open-pit) or *in situ* extraction.[38] In the surface mining method, oil sands ore is mined, crushed, and mixed with a combination of hot water, steam, and caustics (Clark Hot Water Extraction process).[39] While this process can recover approximately 88-95% of the bitumen from the oil sands, a large volume of aqueous waste tailings containing sand, silt, clay, and residual bitumen is produced.[39] These tailings are stored in tailings ponds to facilitate the gravitational separation of the solids from water. As the suspension settles over time, the coarse sand and some of the fine particles settle to the bottom of the pond, while some of the entrapped water is released and is collected at the top of the pond to be recycled.[41] After consolidation for a few years, the tailings settle to about 30-35 wt% solids and are referred to as mature fine tailings (MFT).[39] The fine clay particles in MFT remain dispersed and do not undergo significant consolidation over time due to the electrostatic repulsion between the negatively charged particles. Due to the slow consolidation, MFT require long term storage in tailings ponds. Currently, the ever-growing inventory of tailings ponds in Canada cover an area of over 200 km^2 of land.[42]

In addition to occupying a large area of land, tailings ponds contain large volumes of entrapped water that cannot be recycled for further extraction processes. The long-term storage of tailings also poses several environmental and health concerns, including the

seepage of oil sands process-affected water (OSPW) into surrounding groundwater. Due to the elevated levels of naphthenic acids, inorganics, and metals, seepage of OSPW into groundwater is of concern to nearby communities and wildlife. Additionally, there are environmental concerns over the emission of volatile organic compounds (VOCs) from the tailings ponds.[43] To address these concerns, the Energy Resource Conservation Board in Alberta put in place tailings management regulations for oil sands operators. The objective of these regulations is to ensure that all tailings produced during the life of a project are ready to be reclaimed within ten years after the end of the mining operation.[43–45] While current dewatering technologies can recover about 70% of the water from the oil sands tailings, 3.3 m^3 of tailings are still being produced per 1 m^3 of bitumen extracted. Therefore, if the tailings management regulations are to be met, the existing dewatering technologies need to be improved.[41]

Current commercial methods, such as paste technology, rely on the use of polymer flocculants for the dewatering of MFT.[51] Polymer flocculants are typically long chain water-soluble polymers that can promote the settling of fine particles in colloidal suspensions. When added to a colloidal suspension, if the polymer is of sufficient molecular weight to adsorb onto the surface of more than one particle at the same time, bridging flocculation may occur.[46] Particles linked together via high molecular weight polymers further aggregate to form flocs which can settle by gravity. Most of the commercially available flocculants are polyacrylamide (PAM) based since the polymer is water soluble and can easily be synthesized up to high molecular weights.[46] Additionally, the non-ionic character of PAM can be altered by the incorporation of comonomers. Non-ionic PAM can flocculate suspended particles through the bridging mechanism, where

polymer adsorption occurs through the formation of hydrogen bonds between the acrylamide protons of the polymer and the oxygen atoms on the surface of the clay particles.[41]Anionic polyacrylamides have found promise in the flocculation of oil sands tailings, where the intramolecular electrostatic repulsion between the charged polymer segments causes the polymer chain to adopt an extended conformation. In this extended conformation, the polymer chains can adsorb onto the neutral sites of the clay particles and aggregate via bridging flocculation.[46] The flocculation performance can be improved by first treating the tailings with a coagulant to help overcome the repulsive forces between particles.[41] Cationic polyacrylamides such as the copolymer of acrylamide and diallyl dimethyl ammonium chloride (P(AM-*co*-DADMAC)) have also been explored for the flocculation of oil sands tailings.[51] Cationic PAM can adsorb onto the surface of the negatively charged clay particles by electrostatic attraction. Particles can agglomerate by means of electrostatic interaction between the local positive charge on the surface of the particle and the negative surface charge of another particle.[41]

However, PAM based flocculants result in the formation of loosely packed flocs that retain significant amounts of water due to hydrogen bonding between polymer chains and water molecules. These flocs still need to be contained in tailings ponds and contain a large volume of water that cannot be recycled. Additionally, PAM flocculants have been found to be very effective for the settling of medium and large particles but are not able to remove the smallest particles (< 44 μm).[41] Therefore, the search for a new polymer flocculant specifically designed to overcome these issues is critical to enhance the dewatering performance of polymer flocculants for oil sands tailings. A variety of novel polymers and copolymer have been explored for the flocculation of oil sands tailings.

Polymers such as poly(N-isopropylacrylamide) (PNIPAM) and polyacrylamide/poly(propylene oxide) graft copolymer (PAM-PPO) have been reported to improve the dewatering of oil sands tailings.[52,58,59] The incorporation of a hydrophobic segment in the structure of PAM can improve the dewatering performance by repelling the water trapping in the sediments. Hybrid inorganic/organic materials such as $Al(OH)_3$-polyacrylamide (Al-PAM) have also been investigated for the flocculation of oil sands tailings.[60] The positively charged component of Al-PAM can improve the settling of the very fine particles by means of charge neutralization. Following this, the polyacrylamide chains of Al-PAM promote the aggregation of the particles by flocculation.

In this chapter, the flocculation performance of the activated carbon/polyacrylamide hybrid material (AC-PAM) synthesized in *Chapter 4* is explored. This hybrid material was designed with the intent of combining the functionalities of both the activated carbon and the polymer flocculant, potentially acting in a synergistic manner. Through the incorporation of an activated carbon backbone, it is hypothesized that the flocculation performance of PAM could be enhanced.

5.2 Materials and Methods

5.2.1 Materials

The mature fine tailings (MFT) used for the settling tests were supplied by Suncor Energy Inc. (Alberta, Canada).

5.2.2 Preparation of polyacrylamide (PAM)

Polyacrylamide was synthesized by AGET ATRP as described in *Chapter 4.2.6.*

5.2.3 Preparation of AC-PAM

Polyacrylamide modified activated carbon was synthesized from the oxidation of AC, followed by the attachment of the ATRP initiator, as described in *Chapters 4.2.3* and *4.2.4*. Polyacrylamide was grafted from the surface of AC-BiBB by SI-AGET ATRP, as described in *Chapter 4.2.5*.

5.2.2 Dean-Stark Extraction

The solids, moisture, and bitumen content of the provided MFT sample were determined by Dean-Stark extraction, as described in *Chapter 2.2.1*. Prior to the extraction, the MFT sample was well mixed using a paddle stirrer. Approximately 12.5 g of MFT was placed in a pre-weighed thimble and was hung above a reflux flask containing 200 mL of toluene. As the toluene is refluxed, the vapors evaporate the water from the sample, which both rise to the condenser. The immiscible liquids condense and drip into the trap where they are separated into two layers, with toluene on the top layer. As the toluene in the trap rises to reach the level of the side arm, the toluene drips into the thimble containing the sample. When the toluene flows back into the thimble, the bitumen in the sample is dissolved, which drips back into the flask containing the toluene. The reflux is continued for approximately 24 hours until the solvent dripping from the thimble is visibly free of bitumen. Once the reflux is complete, the thimble is dried in an oven at 110°C overnight and weighed to determine the solid content of the sample. The water from the trap is drained and weighed to determine the moisture content of the sample. Finally, the toluene/bitumen solution is placed in a 250 mL volumetric flask, filled with fresh toluene, and mixed well. 5 mL of the solution was pipetted onto a pre-weighed filter paper and the toluene is allowed to evaporate. Once thoroughly dry, the

filter paper is weighed to determine the mass of bitumen in the 5 mL sample. The mass of bitumen in the sample is obtained from the mass of bitumen in 5 mL multiplied by 20.[52]

5.2.3 Settling Tests

Settling tests were conducted by weighing out 100.0 g of MFT slurry (diluted to 5 wt% solids in deionized water) into a 250 mL beaker. Flocculant dosages are reported as mg of polymer per kg of solids in the MFT. The slurry was mixed at 600 rpm using a three-blade propeller while the flocculant was added. For AC-PAM, the flocculant was added as a powder, while PAM was pre-dissolved in deionized water to a concentration of 0.02 g/mL. After flocculant addition, the suspension was mixed at 600 rpm for 2 minutes, followed by 200 rpm for 8 minutes. The mixture was then transferred to a 100 mL graduated cylinder and the change in height of the mudline was recorded over time. A settling profile was obtained by plotting the mudline height vs. time, and the initial settling rate (ISR) was reported as the slope of the initial linear section of the settling profile. After the slurry was allowed to consolidate for 24 hours, the supernatant was carefully pipetted, and the turbidity was measured using a DR/890 Portable Colorimeter (Hach).[51]

5.2.4 Characterization

AC-PAM was characterized using FTIR, XPS, TGA, and specific surface area, as described in *Chapter 4.3.1.* The molecular weight of AC-PAM and PAM were determined by size exclusion chromatography, also described in *Chapter 4.3.1* and *Chapter 4.3.2.*

5.3 Results and Discussion

5.3.1 Dean-Stark Extraction

Since the flocculation performance of a given flocculant is dependent on the composition of the colloid, it is important to ensure that the composition of this colloid is well known and kept consistent throughout the flocculation tests. As the composition of the received MFT sample is variable from batch to batch, Dean-Stark extraction was used to determine the solid, water, and bitumen content of the given sample. The extraction was repeated in triplicate (Table 5.1) and indicated that the MFT sample contains 36.26 ± 2.46 wt% solids, 57.44 ± 3.18 wt% water, and 6.30 ± 1.18 wt% bitumen. From these results, the MFT sample was diluted to contain 5 wt% solids for settling tests.

Table 5.1 *– Composition of MFT determined from Dean-Stark extraction*

Composition (wt%)	Trial 1	Trial 2	Trial 3	Average
Water	61.07	55.15	56.11	57.44 ± 3.18
Solids	33.47	37.21	38.10	36.26 ± 2.46
Bitumen	5.46	7.64	5.79	6.30 ± 1.18

5.3.2 Flocculation performance

The flocculation performance of AC-PAM was investigated by conducting settling tests to measure the initial settling rate and turbidity of the supernatant after 24 hours of settling. The results were compared to the flocculation performance of PAM with a similar molecular weight to the grafted PAM. PAM was synthesized under the same conditions of AC-PAM, as described in *Chapter 4.* After polymerization for 24 hours, the number-average molecular weight of PAM was measured as 194,300 g/mol with a dispersity value of 2.56. Comparatively, the molecular weight of the grafted polymer

measured after acid catalyzed hydrolysis was found to be 176,100 g/mol with a dispersity value of 2.10.

Since polymer dosage is known to significantly affect the flocculation performance of a given polymer, a variety of dosages were explored for the different flocculants (Table 5.2). Typically, polymer dosage is found to increase the flocculation efficiency for a given polymer up to a certain dosage in which the flocculation is optimized. The optimal dosage for a flocculant is reported to be when there is partial coverage of the particle surface, leaving sufficient unoccupied area for the adsorption of another polymer attached to other particles, thereby facilitating bridging flocculation.[41,58] Beyond the optimal polymer dosage, the particle surface becomes fully covered resulting in decreased flocculation performance.

Table 5.2 *– Initial settling rates and supernatant turbidity for flocculation of 5 wt% MFT with polyacrylamide (PAM) and polyacrylamide modified AC (AC-PAM)*

Sample	Dosage (mg polymer/kg solids)	Initial Settling Rate (m/hr)	Supernatant Turbidity (NTU)
PAM	8,000	2.30	1,350
	10,000	3.51	430
	20,000	2.97	840
AC-PAM	10,000	0.81	5,280
	15,000	0.81	3,320
	20,000	27.54	114
AC	20,000	-	19,700

This trend was observed with the flocculation using PAM, where the optimal polymer dosage for PAM was found to be 10,000 ppm, producing an initial settling rate of 3.51 m/hr and a supernatant turbidity of 430 NTU (Figure 5.1). When the dosage was further increased to 20,000 ppm, over-dosing was observed, and the initial settling rate was reduced to 2.97 m/hr and the supernatant turbidity increased to 840 NTU. At lower

polymer dosages of 8,000 ppm, the flocculation performance was greatly reduced, producing a slower initial settling rate of 2.30 m/hr and a supernatant turbidity of 1350 NTU.

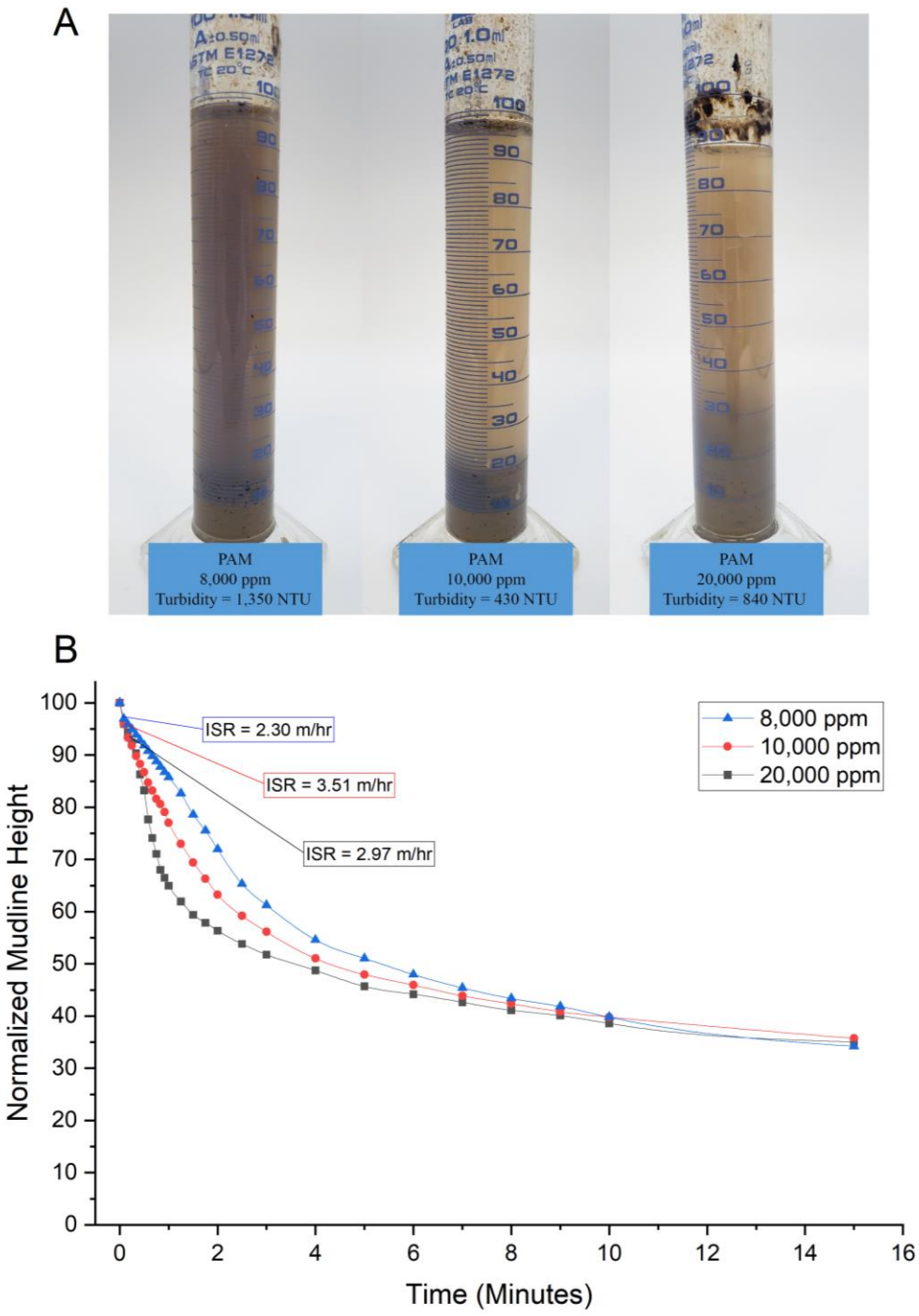

Figure 5.1 *– Settling test results for the flocculation of 5 wt% MFT with various dosages of polyacrylamide (PAM). a) Images of the MFT treated with PAM after settling for 24 hours, b) Settling profiles and initial settling rates (ISR) for the flocculation of MFT with PAM*

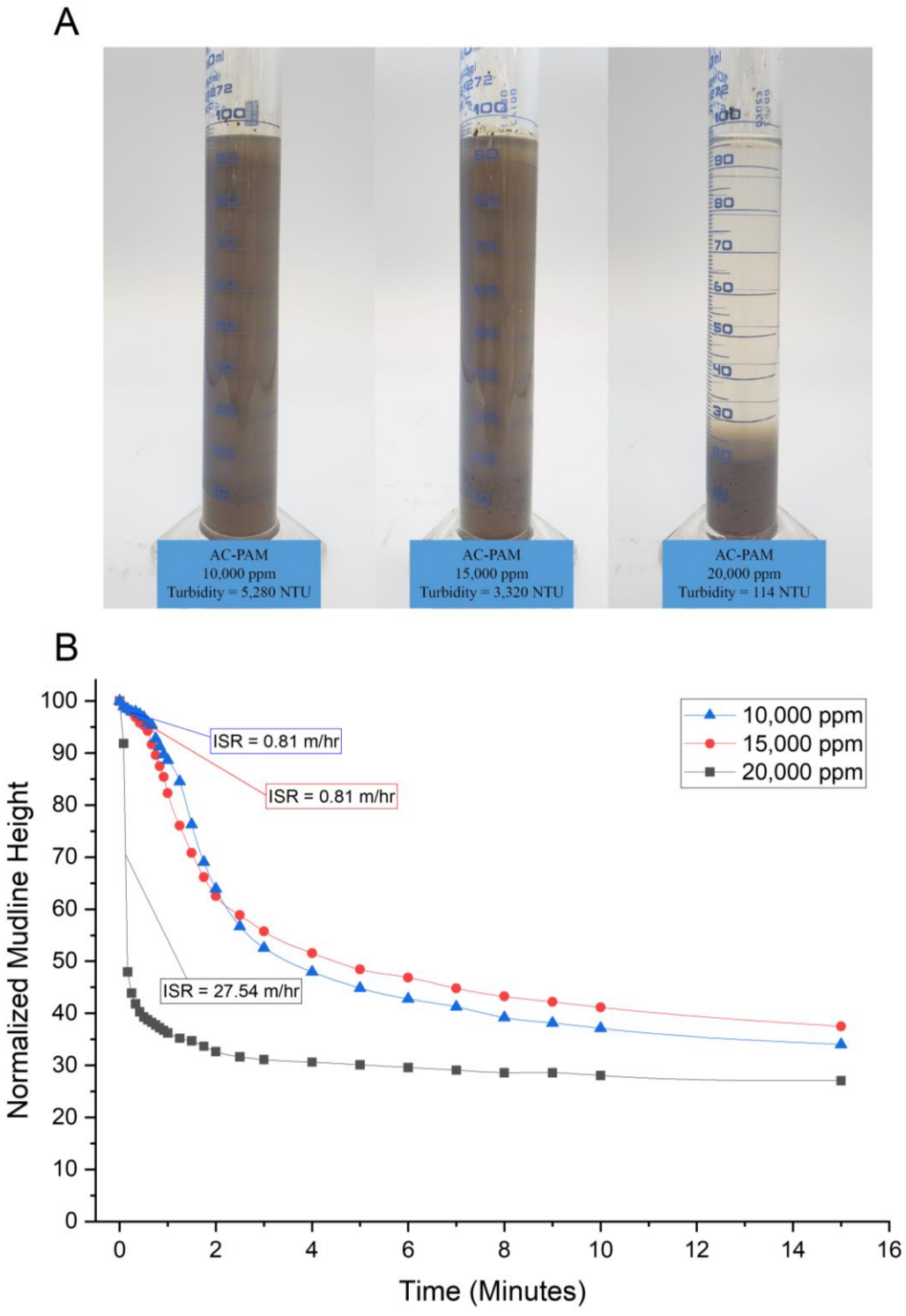

Figure 5.2 *- Settling test results for the flocculation of 5 wt% MFT with various dosages of polyacrylamide modified activated carbon (AC-PAM). a) Images of the MFT treated with AC-PAM after settling for 24 hours, b) Settling profiles and initial settling rates (ISR) for the flocculation of MFT with AC-PAM*

The optimal dosage for the flocculation using AC-PAM was found to be 20,000 ppm. At polymer dosages of 10,000 ppm and 15,000 ppm, the flocculation performance of AC-PAM was greatly reduced. At the optimal dosage, the supernatant turbidity of the released water was 114 NTU and a fast initial settling rate of 27.54 m/hr was measured. Compared to the flocculation results using the optimal dosage of just PAM, the AC-PAM flocculant produced better supernatant turbidity values and faster initial settling rates. However, a larger dosage of AC-PAM of 20,000 ppm was required to produce these results, compared to only 10,000 ppm for PAM. However, the dosage of AC-PAM refers to the total mass of AC-PAM added, not only the PAM polymer content. From the TGA results in the characterization of AC-PAM, it was estimated that the AC-PAM is composed of roughly 10.6% PAM by weight. From this, we can calculate that the 20,000 ppm AC-PAM dosage contains approximately 2,120 ppm of grafted PAM. Now when comparing the flocculation performances of AC-PAM and PAM, AC-PAM was able to produce better flocculation results using a significantly lower polymer dosage. We hypothesize that this occurs due to the increased effective molecular weight of PAM when grafted from the surface of activated carbon. While the molecular weight of the grafted polymer was measured as 176,100 g/mol, this refers to the molecular weight of a single polymer chain on the surface of activated carbon. Presuming multiple polymer chains are attached to a single particle of activated carbon, the polymer should be extended from the surface of activated carbon in 3-dimensions. Therefore, the hydrodynamic radius of AC-PAM should be at least double the hydrodynamic radius of a single polymer chain. Since the flocculation performance of a polymer is influenced by the number of particles that can be adsorbed onto the surface (a function of molecular

weight), AC-PAM should contain more adsorption sites, leading to a better flocculation performance.

5.4 Conclusions

In this chapter, the flocculation performance of PAM and AC-PAM was examined by conducting settling tests. The optimal polymer dosage for PAM was found to be 10,000 ppm, producing an initial settling rate of 3.51 m/hr and a supernatant turbidity of 430 NTU. Comparatively, the optimal dosage for AC-PAM was found to be 20,000 ppm, producing a supernatant turbidity of 114 NTU and a fast initial settling rate of 27.54 m/hr. The improved flocculation performance is hypothesized to occur due to the effective increase in the molecular weight of PAM when grafted from the surface of activated carbon.

6. Conclusions

6.1 General Conclusions

In this work, polyacrylamide (PAM) was successfully grafted from the surface of activated carbon (AC) by surface-initiated activators generated by electron transfer atom transfer radical polymerization (SI-AGET ATRP). Prior to the attachment of the ATRP initiator, the surface of the activated carbon was oxidized to increase the oxygen content, preferentially in the form of phenol functional groups. A variety of oxidants were explored for the pre-functionalization of AC, including HNO_3, H_2O_2, and APS. Additionally, the effect of oxidation time for these three oxidants was examined, as well as the effect of HNO_3 concentration. The surface chemistry of the various oxidized ACs were evaluated by XPS, while the textural characteristics were evaluated by N_2 adsorption. Oxidation by APS for 4 hours was determined as the ideal oxidation conditions for AC, producing an oxidized AC with a relatively conserved surface area and a high content of C-OH/C-O-C functional groups. From the oxidized AC surface, SI-AGET ATRP of acrylamide monomers was performed. The grafting of polyacrylamide from the surface of AC (AC-PAM) was confirmed by characterization with FTIR, XPS, TGA, SEC, and N_2 adsorption. The AC-PAM was measured to contain approximately 10.6% PAM by weight, and the average-number molecular weight of the grafted polymer was 176,100 g/mol with a dispersity value of 2.10. While the characterization results indicated successful grafting of polyacrylamide from the surface of activated carbon, the polymer molecular weight and dispersity values indicate relatively weak control over the polymerization. This was confirmed when investigating the polymerization of acrylamide by AGET ATRP. Subsequent work in this area could focus on improving the ATRP

conditions to create a more controlled polymer architecture. If the conditions are appropriately selected, the polymerization should display first-order kinetics and a linear increase in molecular weight with monomer conversion. If control over the polymerization is achieved, PAM could hopefully be synthesized to higher molecular weight.

The flocculation performance of the hybrid material was explored by conducting settling tests with 5 wt% mature fine tailings (MFT). This was compared to the flocculation performance of PAM synthesized under similar conditions as AC-PAM (M_n = 194,300 g/mol, Đ = 2.56). The optimal polymer dosage for flocculation using just PAM was found to be 10,000 ppm, producing an initial settling rate of 3.51 m/hr and a supernatant turbidity of 430 NTU. Comparatively, the optimal dosage for flocculation using AC-PAM was 20,000 ppm, producing a fast initial settling rate of 27.54 m/hr and a supernatant turbidity of 114 NTU. An AC-PAM dosage of 20,000 ppm was estimated to contain approximately 2,120 ppm of polymer, representing a substantially lower dosage of polymer compared to the pure PAM flocculant. We hypothesize that this occurs due to the increased effective molecular weight of PAM when grafted from the surface of activated carbon.

6.2 Future Work

1. Establishing control over the polymerization of acrylamide by AGET ATRP. This can be achieved by conducting a thorough investigation on the polymerization conditions used, including temperature, reactant ratios, solvent, catalyst, etc. It is important to establish control over the polymerization to give access to higher

molecular weight polymers, as well as the potential for forming block co-polymers.

2. Explore the flocculation and dewatering performance of AC-PAM for the treatment of 35 wt% MFT. This current work only investigated the flocculation performance using 5 wt% MFT. However, if this material is to be used to treat the existing MFT inventory, the flocculation performance for 35 wt% MFT should be investigated. This will require development or adoption of settling tests outside of the usual initial settling rate test.
3. Determine if the AC is simultaneously adsorbing contaminants from the MFT suspension during the flocculation treatment. This could be examined by measuring the total organic carbon content and concentration of metals in the released water after flocculation.
4. Explore the grafting of other polymers from the surface of AC utilizing SI-AGET ATRP for other environmental applications. This method could easily be adapted for the grafting of other polymers that can be synthesized by ATRP. Depending on the polymer identity, the hybrid material could be used to enhance the removal of certain contaminants from solution. For example, the grafting of a quaternary ammonium containing polymer could be used to enhance the chloride removal of AC by anion exchange.

6.3 Contributions to Science

6.3.1 Publications and Patents

- A manuscript for the synthesis and characterization of AC-PAM by SI-AGET ATRP for flocculation applications is currently in preparation

- In collaboration with Dr. Kevin Scotland and Oliver Strong, I worked on a project for the grafting of polyacrylamide through an enol modified activated carbon. This work is currently under review for publication in *The Canadian Journal of Chemical Engineering.*
- Additionally, the work on the grafting of polyacrylamide through an enol modified activated carbon has been filled for a U.S provisional patent in collaboration with Carbonix Inc.
    - Pede, P.R.; Vreugdenhil, A.J.; Strong, O.K.L.; Scotland, K.M.; Bégin, S.J. Functionalized Activated Carbon Products, Processes for Producing Functionalised Activated Carbon Products, and uses of Functionalized Activated Carbon Products. U.S Patent Application No. 63289706. Filed December 15, 2021.

6.3.2 Conferences

- Attended the GrapheneCanada Online 2020 Conference in November 2020
- Oral presentation (virtual) at the Canadian Chemistry Conference and Exhibition (CCCE) in August 2021
    - Received an award for first place in the oral presentations category, water treatment theme in the symposium entitled *Environmental chemistry and Sustainability: a Health intake: Environmental Pollutants in Air, Water, Food, and their Removal*
- Oral presentation at the Canadian Chemistry Conference and Exhibition (CCCE) in June 2022

- Oral presentation at the IUPAC-MACRO 2022 - 49th World Polymer Congress in July 2022
- Oral presentation at the 7th annual International Institute for Environmental Studies (IIES) Science & Policy Workshop and Graduate Student Forum in Vietnam in October 2022

Appendix

Supplementary Figures

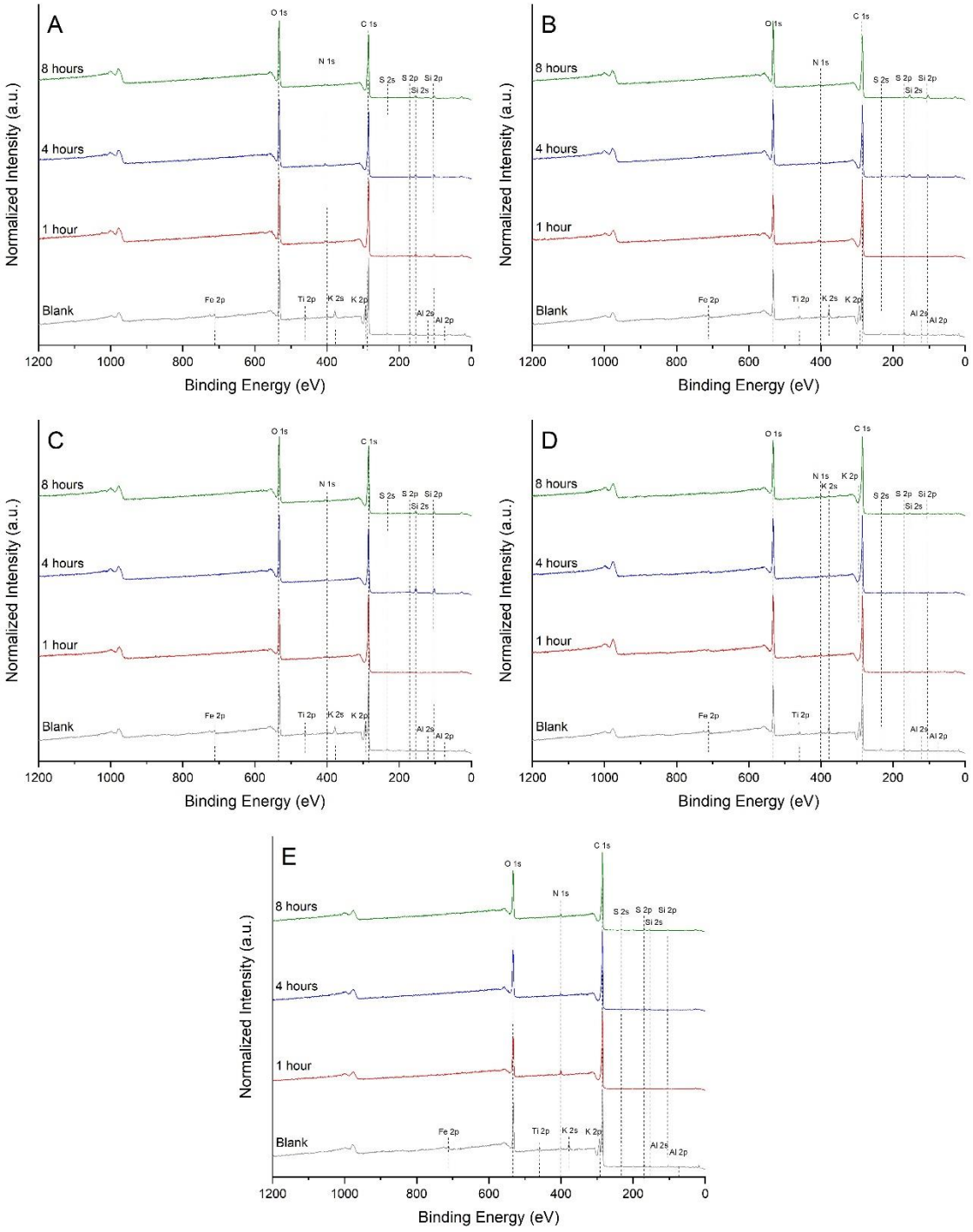

Figure S1 *– XPS Survey scans for oxidized activated carbons with a)15.8 M HNO_3 , b) 10.0 M HNO_3, c) 5.0 M HNO_3 , d) 9.8 M H_2O_2,, and e)2.0 M APS*

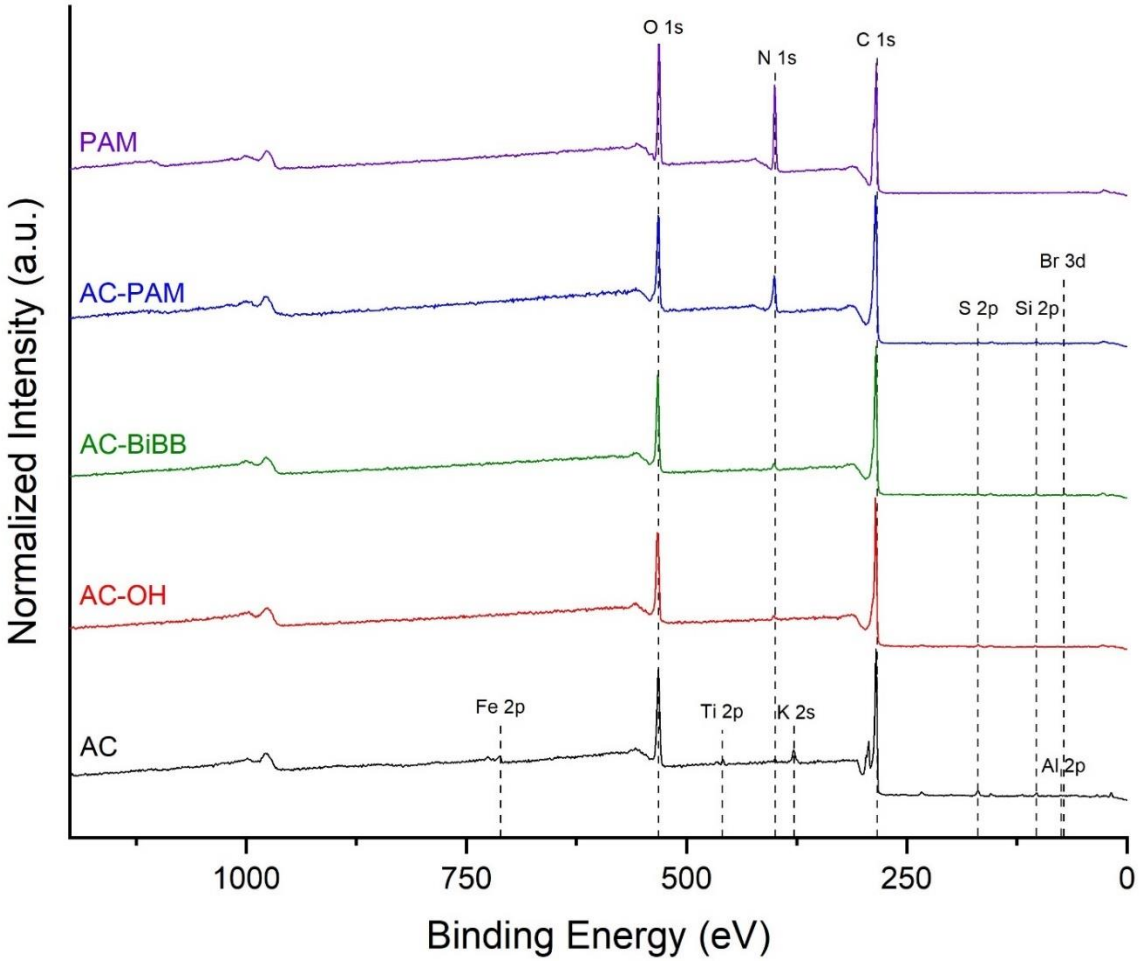

Figure S2 *– XPS survey scans for activated carbon (AC), oxidized AC (AC-OH), ATRP initiator functionalized AC (AC-BiBB), polyacrylamide functionalized AC (AC-PAM), and polyacrylamide (PAM)*

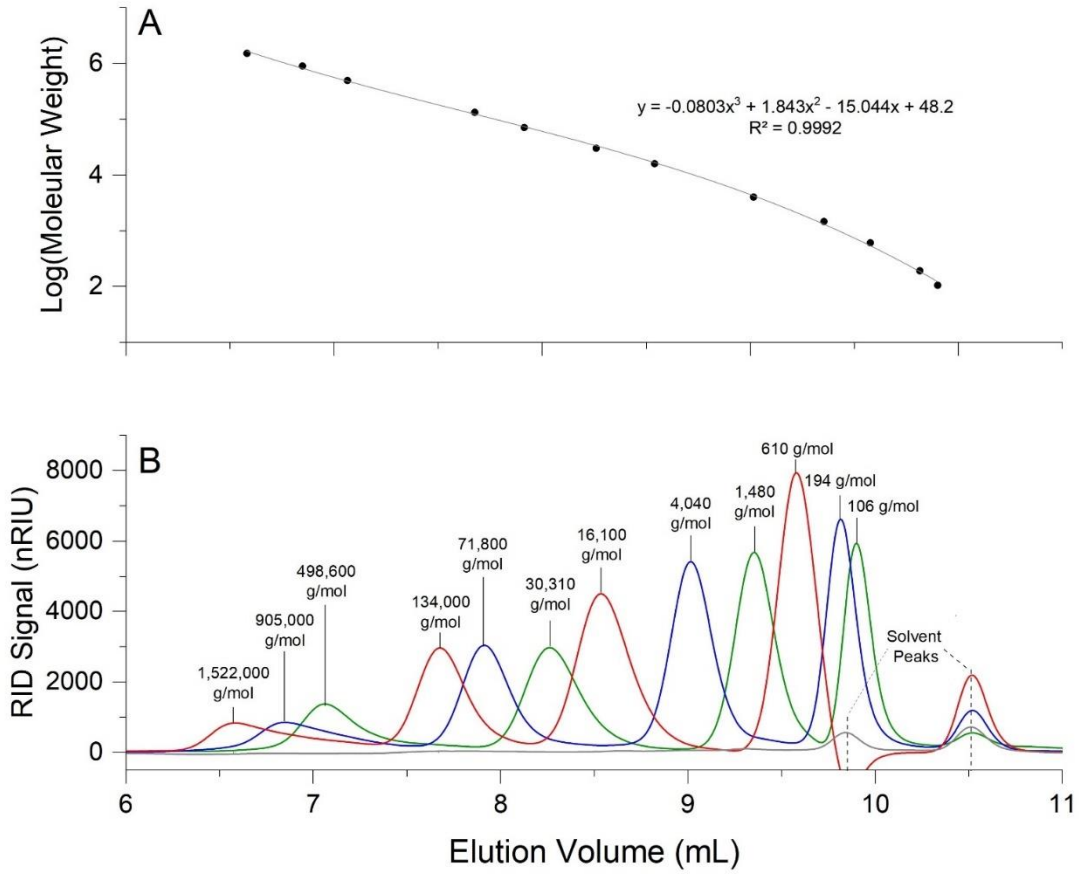

Figure S3 *– a) Calibration curve for SEC chromatography column created from PEO/PEG standards, b) SEC chromatogram for the PEO/PEG standards*

Supplementary Tables

Table S1– *Average BET surface area and standard deviation for unmodified AC and AC oxidized by HNO_3, H_2O_2, and APS*

Conditions		BET Surface Area (m^2/g)	
Treatment	**Time (hrs)**	**Average**	**Standard deviation**
Blank AC	/	716.36	4.46
15.8 M HNO_3	**1**	547.39	50.78
	4	23.70	5.30
	8	34.93	25.94
10.0 M HNO_3	**1**	670.75	20.81
	4	372.43	16.09
	8	143.62	13.26
5.0 M HNO_3	**1**	678.73	28.89
	4	464.68	52.41
	8	326.37	45.49
9.8 M H_2O_2	**1**	566.70	48.83
	4	521.63	15.86
	8	521.70	20.41
2.0 M APS in 1.0 M H_2SO_4	**1**	776.41	13.25
	4	544.69	18.69
	8	495.17	119.94

Table S2 – *% Peak area of C 1s components for unmodified AC, AC-OH, AC-BiBB, AC-PAM, and PAM*

Sample	Peak area of C1s component						
	C=C	**C-C, C-H**	**C-OH, C-O-C**	**C=O**	**O=C-O**	**O=C-N**	**Pi-Pi***
AC	9.86	78.57	5.24	2.68	2.77	-	0.88
AC-OH	5.92	71.94	7.34	3.48	8.50	-	2.82
AC-BiBB	8.06	66.37	9.77	4.75	9.52	-	1.53
AC-PAM	7.75	59.84	9.35	2.34	6.66	9.35	4.71
PAM	-	64.79	-	-	-	35.21	-

Table S3- *% Peak area of N 1s components for AC-PAM and PAM*

Sample	Peak area of N1s component		
	Amide	**Graphitic-N**	**Oxidized-N**
AC-PAM	74.09	21.59	4.32
PAM	100	-	-

References

(1) Marsh, Harry.; Rodríguez-Reinoso, F. *Activated Carbon*, 1st ed.; Elsevier: Amsterdam, 2006.

(2) Bansal, R. C.; Goyal, M. *Activated Carbon Adsorption*, 1st ed.; CRC Press: Boca Raton, 2005.

(3) Celzard, A.; Fierro, V.; Marêché, J. F.; Furdin, G. Advanced Preparative Strategies for Activated Carbons Designed for the Adsorptive Storage of Hydrogen. *Adsorption Science and Technology* **2007**, *25* (3–4), 129–142. https://doi.org/10.1260/026361707782398254.

(4) Everett, D. H. Manual of Symbols and Terminology for Physicochemical Quantities and Units, Appendix II: Definitions, Terminology and Symbols in Colloid and Surface Chemistry. *Pure and Applied Chemistry* **1972**, *31* (4), 577–638. https://doi.org/10.1351/pac197231040577.

(5) Li, N.; Ma, X.; Zha, Q.; Kim, K.; Chen, Y.; Song, C. Maximizing the Number of Oxygen-Containing Functional Groups on Activated Carbon by Using Ammonium Persulfate and Improving the Temperature-Programmed Desorption Characterization of Carbon Surface Chemistry. *Carbon N Y* **2011**, *49*, 5002–5013. https://doi.org/10.1016/j.carbon.2011.07.015.

(6) Lee, M. S.; Park, M.; Kim, H. Y.; Park, S. J. Effects of Microporosity and Surface Chemistry on Separation Performances of N-Containing Pitch-Based Activated Carbons for CO2/N2 Binary Mixture. *Sci Rep* **2016**, *6*, 23224. https://doi.org/10.1038/srep23224.

(7) Daud, W. M. A. W.; Houshamnd, A. H. Textural Characteristics, Surface Chemistry and Oxidation of Activated Carbon. *Journal of Natural Gas Chemistry* **2010**, *19* (3), 267–279. https://doi.org/10.1016/S1003-9953(09)60066-9.

(8) Bhatnagar, A.; Hogland, W.; Marques, M.; Sillanpää, M. An Overview of the Modification Methods of Activated Carbon for Its Water Treatment Applications. *Chemical Engineering Journal* **2013**, *219*, 499–511. https://doi.org/10.1016/j.cej.2012.12.038.

(9) Rivera-Utrilla, J.; Sánchez-Polo, M.; Gómez-Serrano, V.; Álvarez, P. M.; Alvim-Ferraz, M. C. M.; Dias, J. M. Activated Carbon Modifications to Enhance Its Water Treatment Applications. An Overview. *J Hazard Mater* **2011**, *187*, 1–23. https://doi.org/10.1016/j.jhazmat.2011.01.033.

(10) López de la Torre, M. D.; Melguizo Guijarro, M. Covalent Bonds on Activated Carbon. *European J Org Chem* **2010**, 5147–5154. https://doi.org/10.1002/ejoc.201000708.

(11) Zoppe, J. O.; Ataman, N. C.; Mocny, P.; Wang, J.; Moraes, J.; Klok, H. A. Surface-Initiated Controlled Radical Polymerization: State-of-the-Art, Opportunities, and Challenges in Surface and Interface Engineering with Polymer Brushes. *Chem Rev* **2017**, *117*, 1105–1318. https://doi.org/10.1021/acs.chemrev.6b00314.

(12) Chen, W. L.; Cordero, R.; Tran, H.; Ober, C. K. 50th Anniversary Perspective: Polymer Brushes: Novel Surfaces for Future Materials. *Macromolecules* **2017**, *50*, 4089–4113. https://doi.org/10.1021/acs.macromol.7b00450.

(13) Eskandari, P.; Abousalman-Rezvani, Z.; Roghani-Mamaqani, H.; Salami-Kalajahi, M.; Mardani, H. Polymer Grafting on Graphene Layers by Controlled Radical Polymerization. *Adv Colloid Interface Sci* **2019**, *273*, 102021. https://doi.org/10.1016/j.cis.2019.102021.

(14) Bousquet, A.; Awada, H.; Hiorns, R. C.; Dagron-Lartigau, C.; Billon, L. Conjugated-Polymer Grafting on Inorganic and Organic Substrates: A New Trend in Organic Electronic Materials. *Prog Polym Sci* **2014**, *39*, 1847–1877. https://doi.org/10.1016/j.progpolymsci.2014.03.003.

(15) Sakellariou, G.; Priftis, D.; Baskaran, D. Surface-Initiated Polymerization from Carbon Nanotubes: Strategies and Perspectives. *Chem Soc Rev* **2013**, *42*, 677–704. https://doi.org/10.1039/c2cs35226e.

(16) Zhu, B.; Lu, D.; Ge, J.; Liu, Z. Uniform Polymer-Protein Conjugate by Aqueous AGET ATRP Using Protein as a Macroinitiator. *Acta Biomater* **2011**, *7*, 2131–2138. https://doi.org/10.1016/j.actbio.2011.01.033.

(17) Zhou, X.; Liu, X.; Xie, Z.; Zheng, Z. 3D-Patterned Polymer Brush Surfaces. *Nanoscale* **2011**, *3*, 4929–4939. https://doi.org/10.1039/c1nr11238d.

(18) Matyjaszewski, K. Atom Transfer Radical Polymerization (ATRP): Current Status and Future Perspectives. *Macromolecules* **2012**, *45*, 4015–4039. https://doi.org/10.1021/ma3001719.

(19) Young, R. J.; Lovell, P. A. *Introduction to Polymers*, 3rd Edition.; CRC Press: Boca Raton, 2011.

(20) Matyjaszewski, K.; Davis, T. P. *Handbook of Radical Polymerization*; Wiley-Interscience: Hoboken, 2002.

(21) Braunecker, W. A.; Matyjaszewski, K. Controlled/Living Radical Polymerization: Features, Developments, and Perspectives. *Prog Polym Sci* **2007**, *32*, 93–146. https://doi.org/10.1016/j.progpolymsci.2006.11.002.

(22) Corrigan, N.; Jung, K.; Moad, G.; Hawker, C. J.; Matyjaszewski, K.; Boyer, C. Reversible-Deactivation Radical Polymerization (Controlled/Living Radical Polymerization): From Discovery to Materials Design and Applications. *Prog*

Polym Sci **2020**, *111*, 101311. https://doi.org/10.1016/j.progpolymsci.2020.101311.

(23) Qui, J.; Charleux, B.; Matyjaszewski, K. Progress in Controlled/Living Polymerization in Aqueous Media. *Polimery* **2001**, *46*, 453–574.

(24) Krys, P.; Matyjaszewski, K. Kinetics of Atom Transfer Radical Polymerization. *Eur Polym J* **2017**, *89*, 482–523. https://doi.org/10.1016/j.eurpolymj.2017.02.034.

(25) Min, K.; Jakubowski, W.; Matyjaszewski, K. AGET ATRP in the Presence of Air in Miniemulsion and in Bulk. *Macromol Rapid Commun* **2006**, *27*, 594–598. https://doi.org/10.1002/marc.200600060.

(26) Simakova, A.; Averick, S. E.; Konkolewicz, D.; Matyjaszewski, K. Aqueous ARGET ATRP. *Macromolecules* **2012**, *45*, 6371–6379. https://doi.org/10.1021/ma301303b.

(27) Matyjaszewski, K.; Hongchen, D.; Jakubowski, W.; Pietrasik, J.; Kusumo, A. Grafting from Surfaces for "Everyone": ARGET ATRP in the Presence of Air. *Langmuir* **2007**, *23*, 4528–4531. https://doi.org/10.1021/la063402e.

(28) Mines, P. D.; Thirion, D.; Uthuppu, B.; Hwang, Y.; Jakobsen, M. H.; Andersen, H. R.; Yavuz, C. T. Covalent Organic Polymer Functionalization of Activated Carbon Surfaces through Acyl Chloride for Environmental Clean-Up. *Chemical Engineering Journal* **2017**, *309*, 766–771. https://doi.org/10.1016/j.cej.2016.10.085.

(29) Ko, D.; Mines, P. D.; Jakobsen, M. H.; Yavuz, C. T.; Hansen, H. C. B.; Andersen, H. R. Disulfide Polymer Grafted Porous Carbon Composites for Heavy Metal Removal from Stormwater Runoff. *Chemical Engineering Journal* **2018**, *348*, 685–692. https://doi.org/10.1016/j.cej.2018.04.192.

(30) Mines, P. D.; Uthuppu, B.; Thirion, D.; Jakobsen, M. H.; Yavuz, C. T.; Andersen, H. R.; Hwang, Y. Granular Activated Carbon with Grafted Nanoporous Polymer Enhances Nanoscale Zero-Valent Iron Impregnation and Water Contaminant Removal. *Chemical Engineering Journal* **2018**, *339*, 22–31. https://doi.org/10.1016/j.cej.2018.01.102.

(31) Kim, B.; Oh, D.; Kang, S.; Kim, Y.; Kim, S.; Chung, Y.; Seo, Y.; Hwang, Y. Reformation of the Surface of Powdered Activated Carbon (PAC) Using Covalent Organic Polymers (COPs) and Synthesis of a Prussian Blue Impregnated Adsorbent for the Decontamination of Radioactive Cesium. *J Alloys Compd* **2019**, *785*, 46–52. https://doi.org/10.1016/j.jallcom.2019.01.154.

(32) Liu, P.; Wang, T. Surface-Initiated Atom Transfer Radical Polymerization of Hydroxyethyl Acrylate from Activated Carbon Power with Homogenized Surface Groups. *Surface Review and Letters* **2007**, *14* (2), 269–275.

(33) Gong, Z.; Li, S.; Ma, J.; Zhang, X. Synthesis of Recyclable Powdered Activated Carbon with Temperature Responsive Polymer for Bisphenol A Removal. *Sep Purif Technol* **2016**, *157*, 131–140. https://doi.org/10.1016/j.seppur.2015.11.040.

(34) Gong, Z.; Li, S.; Ma, J.; Zhang, X. Self-Flocculated Powdered Activated Carbon with Different Oxidation Methods and Their Influence on Adsorption Behavior. *J Hazard Mater* **2016**, *304*, 222–232. https://doi.org/10.1016/j.jhazmat.2015.10.039.

(35) Liu, P.; Zhang, L. Hyperbranched Aliphatic Polyester Modified Activated Carbon Particles with Homogenized Surface Groups. *Surface Review and Letters* **2007**, *14* (6), 1025–1032.

(36) Liu, Y.; Miao, X.; Zhu, J.; Zhang, Z.; Cheng, Z.; Zhu, X. Polymer-Grafted Modification of Activated Carbon by Surface-Initiated AGET ATRP. *Macromol Chem Phys* **2012**, *213*, 868–877. https://doi.org/10.1002/macp.201100668.

(37) *Alberta Energy Outlook - ST98 Executive Summary*; 2022. www.aer.ca.

(38) Finkel, M. L. The Impact of Oil Sands on the Environment and Health. *Curr Opin Environ Sci Health* **2018**, *3*, 52–55. https://doi.org/10.1016/j.coesh.2018.05.002.

(39) *Oil Sands Tailings Technology Review*; 2010. http://hdl.handle.net/10402/era.17507.

(40) Rao, F.; Liu, Q. Froth Treatment in Athabasca Oil Sands Bitumen Recovery Process: A Review. *Energy Fuels* **2013**, *27*, 7199–7207. https://doi.org/10.1021/ef4016697.

(41) Vedoy, D. R. L.; Soares, J. B. P. Water-Soluble Polymers for Oil Sands Tailing Treatment: A Review. *Canadian Journal of Chemical Engineering* **2015**, *93*, 888–904. https://doi.org/10.1002/cjce.22129.

(42) Gumfekar, S. P.; Vajihinejad, V.; Soares, J. B. P. Advanced Polymer Flocculants for Solid–Liquid Separation in Oil Sands Tailings. *Macromol Rapid Commun* **2019**, *40*, 1800644. https://doi.org/10.1002/marc.201800644.

(43) Saborimanesh, N. Toward Sustainable Remediation of Oil Sands Fine Tailings - A Review. *J Environ Manage* **2021**, *288*, 112418. https://doi.org/10.1016/j.jenvman.2021.112418.

(44) *Directive 074: Tailings Performance Criteria and Requirements for Oil Sands Mining Schemes*; 2009.

(45) *Directive 085: Fluid Tailings Management for Oil Sands Mining Projects*; 2022.

(46) Vajihinejad, V.; Gumfekar, S. P.; Bazoubandi, B.; Rostami Najafabadi, Z.; Soares, J. B. P. Water Soluble Polymer Flocculants: Synthesis, Characterization, and Performance Assessment. *Macromol Mater Eng* **2019**, *304*, 1800526. https://doi.org/10.1002/mame.201800526.

(47) Gregory, J.; Barany, S. Adsorption and Flocculation by Polymers and Polymer Mixtures. *Adv Colloid Interface Sci* **2011**, *169*, 1–12. https://doi.org/10.1016/j.cis.2011.06.004.

(48) Stevie, F. A.; Donley, C. L. Introduction to X-Ray Photoelectron Spectroscopy. *Journal of Vacuum Science & Technology A* **2020**, *38*. https://doi.org/10.1116/6.0000412.

(49) Sing, K. S. W.; Everett, D.; Haul, R. A. W.; Moscou, L.; Pierotti, R. A.; Rouquérol, J.; Siemieniewska, T. Reporting Physisorption Data for Gas/Solid Systems with Special Reference to the Determination of Surface Area and Porosity. *Pure and Applied Chemsitry* **1985**, *57* (4), 603–619.

(50) Thommes, M.; Kaneko, K.; Neimark, A. v.; Olivier, J. P.; Rodriguez-Reinoso, F.; Rouquerol, J.; Sing, K. S. W. Physisorption of Gases, with Special Reference to the Evaluation of Surface Area and Pore Size Distribution (IUPAC Technical Report). *Pure and Applied Chemistry* **2015**, *87* (9–10), 1051–1069. https://doi.org/10.1515/pac-2014-1117.

(51) Vajihinejad, V.; Guillermo, R.; Soares, J. B. P. Dewatering Oil Sands Mature Fine Tailings (MFTs) with Poly(Acrylamide-Co-Diallyldimethylammonium Chloride): Effect of Average Molecular Weight and Copolymer Composition. *Ind Eng Chem Res* **2017**, *56*, 1256–1266. https://doi.org/10.1021/acs.iecr.6b04348.

(52) Reis, L. G.; Oliveira, R. S.; Palhares, T. N.; Spinelli, L. S.; Lucas, E. F.; Vedoy, D. R. L.; Asare, E.; Soares, J. B. P. Using Acrylamide/Propylene Oxide Copolymers to Dewater and Densify Mature Fine Tailings. *Miner Eng* **2016**, *95*, 29–39. https://doi.org/10.1016/j.mineng.2016.06.005.

(53) Yan, C. N.; Liu, Q.; Xu, L.; Bai, L. P.; Wang, L. P.; Li, G. Photoinduced Metal-Free Surface Initiated ATRP from Hollow Spheres Surface. *Polymers (Basel)* **2019**, *11* (4), 599. https://doi.org/10.3390/polym11040599.

(54) Jaramillo, J.; Álvarez, P. M.; Gómez-Serrano, V. Oxidation of Activated Carbon by Dry and Wet Methods Surface Chemistry and Textural Modifications. *Fuel Processing Technology* **2010**, *91*, 1768–1775. https://doi.org/10.1016/j.fuproc.2010.07.018.

(55) Ternero-Hidalgo, J. J.; Rosas, J. M.; Palomo, J.; Valero-Romero, M. J.; Rodríguez-Mirasol, J.; Cordero, T. Functionalization of Activated Carbons by HNO3 Treatment: Influence of Phosphorus Surface Groups. *Carbon N Y* **2016**, *101*, 409–419. https://doi.org/10.1016/j.carbon.2016.02.015.

(56) Moreno-Castilla, C.; Ferro-García, M. A.; Joly, J. P.; Carrasco-Marín, F.; Rivera-Utrilla, J. Activated Carbon Surface Modifications by Nitric Acid, Hydrogen Peroxide, and Ammonium Peroxydisulfate Treatments. *Langmuir* **1995**, *11*, 4386–4392.

(57) Fan, Y.; Boulif, N.; Picchioni, F. Thermo-Responsive Starch-g-(PAM-Co-PNIPAM): Controlled Synthesis and Effect of Molecular Components on Solution Rheology. *Polymers (Basel)* **2018**, *10*, 92. https://doi.org/10.3390/polym10010092.

(58) Zhang, D.; Thundat, T.; Narain, R. Flocculation and Dewatering of Mature Fine Tailings Using Temperature-Responsive Cationic Polymers. *Langmuir* **2017**, *33*, 5900–5909. https://doi.org/10.1021/acs.langmuir.7b01160.

(59) Gumfekar, S. P.; Soares, J. B. P. A Novel Hydrophobically-Modified Polyelectrolyte for Enhanced Dewatering of Clay Suspension. *Chemosphere* **2018**, *194*, 422–431. https://doi.org/10.1016/j.chemosphere.2017.12.009.

(60) Yang, W. Y.; Qian, J. W.; Shen, Z. Q. A Novel Flocculant of Al(OH)3-Polyacrylamide Ionic Hybrid. *J Colloid Interface Sci* **2004**, *273*, 400–405. https://doi.org/10.1016/j.jcis.2004.02.002.